Effect of Curing Regime on Properties of Geopolymer Mixtures Containing Basic Oxygen Furnace Slag (BOFS) Aggregates

Zarina Onopriyenko, Bachelor of Engineering

Submitted in fulfilment of the requirements
for the degree of Master of Science
in Civil & Environmental Engineering

School of Engineering and Digital Sciences
Department of Civil & Environmental Engineering
Nazarbayev University

53 Kabanbay Batyr Avenue,
Astana, Kazakhstan, 010000

Supervisors: Chang-Seon Shon

Date of completion: March 15, 2024

Declaration

I, Zarina Onopriyenko, hereby, declare that this manuscript, entitled “Effect of Curing Regime on Properties of Geopolymer Mixtures Containing Basic Oxygen Furnace Slag (BOFS) Aggregates”, is the result of my own work except for quotations and citations which have been duly acknowledged.

I also declare that, to the best of my knowledge and belief, it has not been previously or concurrently submitted, in whole or in part, for any other degree or diploma at Nazarbayev University or any other national or international institution.

Zarina Onopriyenko

March 2024

Abstract

Basic oxygen furnace slag (BOFS) is a by-product material from the steel industry, which might be used as a substitute for the natural aggregates in the construction industry. The issue pertaining to the use of BOFS as an aggregate is the volume expansion in the concrete matrix by $Ca(OH)_2$ (calcium hydroxide) or $Mg(OH)_2$ (magnesium hydroxide) formed by free calcium oxide (f-CaO) and free magnesium oxide (f-MgO) components in BOFS. Mineral sequestration (CO_2 curing) and the geopolymerization technique are potential remedies for the BOFS expansion problem. This research studied the mechanical, durability, and microstructural characteristics of BOFS-based geopolymer mortar under different curing regimes and durations. While flowability and air content are among the fresh properties of geopolymer mixtures, compressive strength, dielectric constant, drying shrinkage, and expansion (1M NaOH solution and water expansion) are the primary focus of the hardened properties and durability of geopolymer mixtures. Scanning electron microscope (SEM) image, Fourier transform infrared (FTIR) spectroscopy, and X-ray diffraction (XRD) analysis were carried out to investigate the microstructural properties of geopolymer mortar.

Four different curing regimes were evaluated: air, water, steam, and combined steam and CO_2 curing. It was looked into how various curing times affected the characteristics of the geopolymer mortar based on BOFS: 6- and 12-hours steam curing and 6-, 12- and 24-hours combined steam and CO_2 curing. Additionally, three different BOFS/Sand ratios of 100/0, 75/25, and 50/50 were compared. The test methods started with evaluating the mortar's fresh properties: flowability and air content.

The fresh property test results indicate that the mixture with a BOFS/Sand ratio of 75/25 has high flowability, and the air content of mortar mixtures increases with the decrease of BOFS content. Furthermore, compressive strength results indicate that steam curing and combined steam and CO_2 curing increase the compressive strength and have a higher dielectric constant value in comparison to ambient air-cured BOFS-based geopolymer mortar. BOFS/Sand ratio of 75/25 and the longer steam and CO_2 curing favored the compressive strength development. However, the BOFS/Sand ratio and duration of steam curing and CO_2 curing do not significantly affect the dielectric constant value.

For drying shrinkage and 1M NaOH and water expansion tests, both steam curing and the combined steam and CO_2 curing hindered the excessive drying shrinkage and expansion in 1M NaOH solution compared to air or water-cured mixtures. The water and 1M NaOH expansion characteristic curves underwent less fluctuation for longer steam and CO_2 curing

duration. The drying shrinkage was favored by longer steam curing duration. However, it was not affected by CO_2 curing duration.

FTIR spectroscopy, SEM image analysis and XRD results indicated that the geopolymerization of the mixture was more apparent during the steam curing and CO_2 curing in comparison to water curing and air curing regimes. The longer duration of steam and CO_2 curing also promoted the formation of more stable and dense geopolymer matrix structure, due to longer hydration and formation of stable carbonate compounds.

Acknowledgments

I want to sincerely thank and appreciate everyone who helped me finish my master's thesis.

First and foremost, I owe a debt of gratitude to Associate Professor Chang-Seon Shon, who provided me with steadfast support, invaluable advice, and insightful guidance throughout the complete process of conducting research. Their expertise and assistance have been invaluable in shaping the direction of this work.

I extend my heartfelt gratitude to all the professors who have played a significant role in shaping my academic journey and the completion of this master's thesis.

I want to express appreciation to my family for their solid understanding and support during this academic journey's difficult moments. Their support and affection have served as my rock-solid foundation.

Finally, I am appreciative of my friends and colleagues from GRIP Lab for their insightful advice and unwavering support in fostering a stimulating and cooperative learning environment.

I am deeply grateful to these people for their contributions to my academic and personal development, as this thesis is the result of their combined efforts and encouragement.

Table of Contents

Declaration 2
Abstract 3
Acknowledgements 5
List of Abbreviations 8
List of Figures 9
List of Tables 11
Chapter 1 - Introduction 12
1.1.Research Background 12
1.2. Research Objectives 13
1.3. Thesis structure 13
Chapter 2 - Literature Review 15
2.1. OPC concrete effect on environment 15
2.2. BOFS 15
2.3. The use of BOFS in concrete 17
2.4. Geopolymers 18
2.4.1. Geopolymerization 19
2.4.2. Source materials 19
2.4.3. Mixture proportions 22
2.5. Curing Regimes 24
2.5.1. Steam curing 24
2.5.2. Ambient air curing 25
2.5.3. Water curing 26
2.5.4. Carbonation/Mineral Sequestration 27
2.6. Properties of BOFS-based geopolymer 29
Chapter 3 - Experimental Program 34
3.1. Materials 34
3.1.1. Binders 34
3.1.2. Aggregates 38
3.1.3. Alkaline Activators 42
3.2. Mixture Proportions 42
3.3. Mixing and Casting 43
3.4. Curing 45
3.5. Testing Procedures 46
3.5.1. Flowability test 46
3.5.2. Air content test 47
3.5.3. Compressive strength test 48
3.5.3. Dielectric constant test 49
3.5.5. Drying shrinkage test 49
3.5.6. 1 M NaOH and Water expansion test 50
3.5.7. X-ray diffraction (XRD) 51
3.5.8. Scanning electron microscope (SEM) image 52
3.5.9. Fourier transform infrared spectroscopy (FTIR) analysis 53

Chapter 4 - Results and Discussion 54
4.1. Fresh Properties 54
4.1.1. Flowability test 54
4.1.2. Air content test 55
4.2. Hardened Properties 56
4.2.1. Compressive strength 56
4.2.2. Dielectric constant 58
4.3. Durability 61
4.3.1. Shrinkage strain 61
4.3.2. 1M NaOH expansion and water expansion 64
4.4. Microstructural Properties 66
4.4.1. X-ray diffractometer (XRD) investigation 66
4.4.2. Scanning Electron Microscope (SEM) image analysis 67
4.4.3. Fourier transform infrared spectroscopy (FTIR) analysis 69
Chapter 5 - Conclusion 71
References 74
Appendix 83

List of Abbreviations

AAS	Alkali activated solution
AC	Absorption capacity
ASR	Alkali-silica reaction
ASTM	American Society for Testing and Materials
BF(S)	Blast furnace (slag)
BOFS	Basic Oxygen Furnace slag
C-A-S-H	Calcium Alumino Silicate hydrate
C-S-H	Calcium Silicate hydrate
EDS	Energy dispersive X-ray spectroscopy
FA	Fly ash
FTIR	Fourier transform infrared spectroscopy
GGBFS	Ground granulated blast furnace slag
LF	Ladle furnace
N-A-S-H	Sodium aluminoscshilicate hydrate
OPC	Ordinary Portland cement
PSD	Particle size distribution
SEM	Scanning electron microscopy
SG	Specific Gravity
XRD	X-ray diffraction
XRF	X-ray fluorescence

List of Figures

Figure 2.1: The effect of carbonization time on compressive strength [91] 28
Figure 2.2: Comparison of compressive strength value at different ages [92] 29
Figure 3.1: Procedure of determining SG of binder materials 35
Figure 3.2: Mastersizer 3000 36
Figure 3.3: PSD of binder materials 36
Figure 3.4: XRF equipment 37
Figure 3.5: Crystalline phases of FA 38
Figure 3.6: Crystalline phases of GGBFS 38
Figure 3.7: Procedure of determining SG and AC of aggregate materials 40
Figure 3.8: Crystalline phases of BOFS 41
Figure 3.9: Crystalline phases of GGBFS 41
Figure 3.10: Hobart mixer (4.7 L) 44
Figure 3.11: Steam curing chamber and steam generator 46
Figure 3.12: Carbonization chamber 46
Figure 3.13: Flow table test 47
Figure 3.14: Cylindrical unit measure (400 ml) 48
Figure 3.15: (a)Compression and bending testing machine of concrete samples; (b)samples with 50x50x50 mm dimensions 48
Figure 3.16: (a)Dielectric constant test equipment and software; (b)samples with 70x70x70 mm dimensions 49
Figure 3.17: (a)Comparator with digital display for measuring drying shrinkage (ASTM C596) and scales; (b)samples with 285x25x25 mm dimensions 50
Figure 3.18: (a)comparator with digital display for measuring expansion (ASTM C1260), (b)samples with 285x25x25 mm dimensions 51
Figure 3.19: (a)X-ray diffreaction equipment; (b)geopolymer powder samples 52
Figure 3.20: (a)SEM apparatus; (b)coating equipment 52
Figure 3.21: (a)Nicolet FTIR Spectrometer 53
Figure 4.1: Relative flowability test results of geopolymer mortar mixtures 54
Figure 4.2: Air content of geopolymer mortar mixtures 55
Figure 4.3: Compressive strength (a) Steam curing 6 hours; (b) Steam curing 12 hours 56
Figure 4.4: Compressive strength (a) Ambient air curing; (b) Water curing 57
Figure 4.5: Compressive strength (a) 6hr Steam + 6,12,24hr CO_2 curing; (b) 12hr Steam + 6,12,24hr CO_2 curing 58
Figure 4.6: Dielectric constant (a) Steam curing 6 hours; (b) Steam curing 12 hours 59
Figure 4.7: Dielectric constant (a) Ambient air curing; (b) Water curing 60
Figure 4.8: Dielectric constant (a) 6hr Steam + 6,12,24hr CO_2 curing; (b) 12hr Steam + 6,12,24hr CO_2 curing 60
Figure 4. 9: Drying shrinkage length loss (%) (a) Steam curing 6 hours; (b) Steam curing 12 hours 61
Figure 4. 10: Drying shrinkage mass loss (%) (a) Steam curing 6 hours; (b) Steam curing 12 hours 62
Figure 4. 11: Drying shrinkage length loss (%) (a) Ambient air curing; (b) Water curing 63

Figure 4. 12: Drying shrinkage mass loss (%) (a) Ambient air curing; (b) Water curing..... 63
Figure 4. 13: Drying shrinkage length loss (%) (a) 6hr Steam + 6,12,24hr CO_2 curing; (b) 12hr Steam + 6,12,24hr CO_2 curing 64
Figure 4. 14: Drying shrinkage mass loss (%) (a) 6hr Steam + 6,12,24hr CO_2 curing; (b) 12hr Steam + 6,12,24hr CO_2 curing 64
Figure 4. 15: 1M NaOH expansion 65
Figure 4. 16: Water expansion 66
Figure 4. 17: XRD pattern of (a) Steam cured 6hr and (b) Steam cured 12hr samples 67
Figure 4. 18: SEM image of 6h steam cured sample 68
Figure 4. 19: SEM image of ambient air cured sample..... 68
Figure 4. 20: SEM image of water cured sample 69
Figure 4. 21: FTIR spectra 70
Figure 1: XRD pattern of (a) Ambient air and (b) Water cured samples..... 83
Figure 2: XRD pattern of (a) Steam cured 6hr + 6hr CO_2 and (b) Steam cured 6hr + 12hr CO_2 cured samples 83

List of Tables

Table 2.1: Chemical composition of BOFS in %weight 17
Table 3. 1. Specific gravity values of binder materials 34
Table 3. 2. Chemical Composition of FA and GGBFS 37
Table 3. 3. Grading Requirement 39
Table 3. 4. Specific gravity and absorption capacity values of aggregate materials 40
Table 3. 5. Chemical Composition of BOFS and Sand 40
Table 3. 6. Mix design parameters 43
Table 3. 7. Final mix designs (kg/m³) 43
Table 3. 8: Quantity of samples and mixture volume estimation 45
Table 4. 1: EDS results 69

Chapter 1 - Introduction

1.1.Research Background

Geopolymer is an alkali-activated construction material with similar mechanical characteristics to materials made of ordinary Portland cement (OPC) [1]. Typically, binders from industrial waste products such as slag and fly ash (FA) as well as naturally occurring pozzolan like metakaolin, are used to create geopolymers. For the purpose of producing a gel-like substance and for activating the raw materials to produce geopolymer paste, the binders are subjected to resilient alkaline activators including sodium silicate (Na_2SiO_3), potassium hydroxide (KOH) and sodium hydroxide (NaOH) [2]. During the geopolymerization reaction, The formation of the three-dimensional aluminosilicates network framework adds to the remarkable mechanical, fire, and chemical resilience of geopolymer [3]. Thus, geopolymer is considered to be an environmentally friendly construction material that utilizes industrial by-wastes and exhibits outstanding mechanical properties.

Accumulation of industry by-products in landfills threatens the surrounding environment. The steel industry is one of the sectors that produces a significant amount of byproducts. Different types of steel slags are produced in the process of conversion of iron into steel in several furnaces such as a blast furnace (BF), a basic oxygen furnace (BOF), and a ladle furnace (LF). After the BOF is oxygenated, a by-product known as BOF slag (BOFS) is produced. Using steel slags (BF slag (BFS), BOFS, and LF slag (LFS)) effectively in construction materials could positively impact the economy and the surroundings [4]. However, the recent study [5] shows that the presence of free magnesium oxide (f-MgO) and free calcium oxide (f-CaO) in the components of BOFS might cause severe expansion problems during its utilization process. Since f-CaO and f-MgO have low reactivity, their hydration process might undergo after a long period. To overcome the volume instability problem of BOFS, the BOFS is used in its fineness size, and as a result, the hydration process of this material is accelerated.

There are two possible solutions that exist for overcoming the BOFS expansion issue are applying geopolymerization technique and mineral sequestration. Free silicon which leaves unreacted during the geopolymerization and f-CaO and f-MgO reacts to form stable compounds [6]. Wollastonite ($CaSiO_3$) and enstatite ($MgSiO_3$) are formed which prevent the expansion of the BOFS.

$$f\text{-}CaO + Si \rightarrow CaSiO_3 \quad (1.1)$$

$$f\text{-}MgO + Si \rightarrow MgSiO_3 \quad (1.2)$$

Pan et al. [7], studied the effect of the carbonization process on stabilization of BOFS. It is discovered that the BOFS component contains f-CaO and f-MgO that undergo the reaction process with CO_2 during carbonization process and forms stable and insoluble compound such as calcium carbonate ($CaCO_3$).

$$f\text{-}CaO + CO_2 \rightarrow CaCO_3 \quad (1.3)$$

$$f\text{-}MgO + CO_2 \rightarrow MgCO_3 \quad (1.4)$$

Moreover, the implication of steel slag as an admixture is beneficial for developing mechanical and microstructural properties of concrete, as it is rich in mineral composition, containing silicate, aluminum, and calcium [8]. Nonetheless, grinding the steel slag to the fine powder form is economically ineffective due to its toughness. Thus, using steel slag as an aggregate is a more practical, affordable, and assuring approach [9].

1.2. Research Objectives

Much investigation has been conducted on identifying the physical, durability and microstructural properties of BOFS-based geopolymers. On the other hand, not much research has been done regarding how different curing regimes affect the characteristics of geopolymer based on BOFS. Furthermore, the mixed use of BOFS aggregate and natural aggregate in the manufacturing of geopolymer mixture is not well known. The aim of this research project is to investigate the effects on the characteristics of BOFS-based geopolymer of varying curing regimes, aggregate composition of BOFS aggregate, and natural river sand in varying amounts.

1.3. Thesis structure

There are 5 chapters in the Master's Thesis report. The first chapter primarily focuses on the background information of the related topic. Specifically, it is about existing research problems and their possible solutions. The first chapter also outlines the master thesis's overall structure and the extent of this work. Review of the Literature is the second chapter. Understanding the geopolymerization and application of BOFS aggregate, in addition to the influence of particular variables on the evolution of the mechanical, microstructural, and

durability properties of the geopolymer, is largely dependent on the second chapter. The first and second chapter of the work more focused on the theoretical part of research investigation.

The third and fourth chapter include the practical part of the master thesis work. In the third chapter the process of practical work is described as mixing, casting, and curing processes. Additionally, the raw material characterization is included in the third chapter. The fourth chapter focuses on describing the results obtained from practical work, as well as analyzing and comparing the results.

The fifth chapter serves as a conclusion, summarizing the main conclusions of the research project, outlining its shortcomings, and outlining potential avenues for future research.

Chapter 2 - Literature Review

2.1. Ordinary portland cement concrete effect on the environment

The risk of global warming is a major issue threatening modern society. The cause of global warming is greenhouse gas, the emission of carbon dioxide (CO_2). Anthropogenic actions such as burning fossil fuels, deforestation, and others cause CO_2 emissions to the atmosphere. Manufacturing of cement, which is the main component of Ordinary Portland cement (OPC) concrete, is another cause of CO_2 formation. Cement is extensively utilized as a construction material all around the earth. Concrete is a combination of coarse and fine aggregate material, cement, and water. Cement is produced in almost all countries due to its importance in construction and geographical abundance. There are two main processes during which carbon dioxide is produced. First, the operation of a rotary kiln requires the ignition of hydrocarbon deposits. Second is the decarbonization action of limestone, which is one of the main sources of cement. The process is initiated at a temperature of 900 ℃ [10].

$$CaCO_3 \rightarrow CaO + CO_2\uparrow \quad (2.1)$$

In combination, these two processes generate an overall 1.25 tons of CO_2 per ton of cement [11]. Each year, the carbon dioxide emission from the cement industry devotes up to 7% of entire CO_2 emission to the atmosphere worldwide [12]. According to McCaffrey [13], cement production increases by 3% each year, which might be the reason for the rise in global temperature.

2.2. BOFS

Many countries' economies heavily depend on steel and iron manufacturing industries. They supply the fundamental components required for the construction and upkeep of various demands of daily life. Such as city infrastructures, automobiles, houses, factories, and many other structures [14]. In the past decade, the production of steel was approximately 500 million tons per year [15]. However, the steel production by 2015 was estimated to be 1599.5 million tons, which shows an increase in steel production by approximately 200%. By 2016, the number rose to 1666.2 million tons; thus, the rise in steel production in one year was 4%.

China, Japan, and India are some countries with large steel-producing industries [16], responsible for by-product generation, carbon dioxide emission, and energy consumption. The solid waste generated from the steel production industry is also called steel slag. Over 160

million tons of by-products from the steel industry originate annually [17]. Steel slag is a leftover crop which is collected after the metal is smelted and detached from the ore's basic material [18]. Different steel slags exist, which can be classified by their generated process. Advanced countries such as France, Japan, and Germany found several ways of utilizing the steel slag, where the reutilization of it is close to 100%. In 2010, half of the steel produced worldwide corresponds to China, but the steel slags generated simultaneously were not utilized or reused.

The two major slags produced during steel production are the basic oxygen furnace (BOF) slag and blast furnace (BF) slag. The initial step of steel production is the basic oxygen furnace, which also integrates a blast furnace. The upper section of the furnace provides the BF with raw materials like limestone, fuel, and iron ore, while the lower section provides the heat [19]. The final products obtained from the blast furnace are slag and molten metal. Molten metal proceeds into BOF, while the slag is disposed of as a by-product material which is referred to as blast furnace slag (BFS). The BOF is an important step in the steelmaking process to decrease the carbon content of steel [20]. The oxygen is supplied to BOF, where the metal oxidation process takes place, and basic oxygen furnace slag (BOFS) is collected separately from the liquid steel. After the BOFS is collected, it is transferred to casting or processing facilities and disposed of or stored for further use [21]. The steelmaking industry has applied this process for over 20 years, and no significant changes have been applied [22].

The chemical composition of BOFS dramatically varies from place to place, as well as the period when it is collected. The main reason for the varying tendency of BOFS composition is the variability of raw material of the ore and different chemical transformations that result during the steelmaking process [23]. Commonly, the alkalinity ratio of BOFS is high due to the innate properties of the ore source [21]. The basicity of BOFS is apparent in the compounds such as magnesium oxide (MgO) and calcium oxide (CaO) [24]. CaO is one of the affluent compositions in BOFS, followed by iron oxide and silicon dioxide, as shown in Table 2.1.

Depending on the cooling process, BOFS can be classified into 3 different structures: liquid, glassy, and crystalline [25]. Crystalline BOFS is formed during the slow cooling, while a glassy structure is obtained during the tempering. During the slow curing processes, the BOFS particle size tends to be lower than 100 mm [26]. Water-cooled and air-cooled BOFS differ in terms of their density and porosity. The former has low density and high porosity, while the latter has high density and low porosity [27]. The mean values of water absorption capacity and specific gravity of BOFS are 1-1.18% and 3.29 g/cm^3, respectively [28].

Identifying the physical properties of the BOFS is relevant, as it determines the potential of application of the BOFS in the construction material sphere.

Table 2.1: Chemical composition of BOFS in %weight

	China [29]	India [27]
Fe_2O_3	17.8	16.50
Al_2O_3	6.8	1.07
CaO	45.4	50.70
MgO	7.3	10.31
MnO	-	1.05
SiO_2	13.7	17.69
TiO_2	-	-

2.3. The use of BOFS in concrete

BOFS is utilized as an aggregate and binder material for manufacturing concrete. The usage of BOFS is beneficial in economic and environmental aspects. Most of the by-products from the steel industry are disposed of in landfills, causing soil and surrounding environment pollution. Also, the BOFS application reduces the cost of storage, which is required to store slag material, and reduces the energy cost required for material production (cement). Generally, around 5 to 10% of BOFS per ton is reused as a binder material for concrete production [30]. The mechanical properties of BOFS identify how well it is suitable to be the binder material. The chemical composition of BOFS defines the mechanical properties. According to Altun and Yılmaz [31], the compressive strength and bending strength values of 2-, 7- and 28-day concrete made with 100% cement and 70% cement + 30% BOFS are comparatively the same. Since the high content of MgO in the component of BOFS delays the hydration process and lengthens the setting time of concrete, BOFS with a lower content of MgO is preferable [31]. The BOFS in the concrete compound was found to change the physicochemical properties of the concrete. Research conducted by Calmon et al. [32] found that the BOFS as a binder decreases the water amount required to initiate the flowability of the cement paste.

According to Ding et al. [33], finding alternative materials is vital because almost 15 million tons of natural aggregates are utilized yearly for concrete production. Concrete, along with steel, is one of the most consumed construction materials worldwide. Thus, using natural stone as an aggregate in large quantities threatens the environment as the process of mining and transporting requires fuel combustion and causes dust distribution. Since about 75% of concrete components comprise aggregates, the properties of aggregate material influence

concrete's mechanical and durability properties. BOFS and other industrial by-products are suitable substitutes for natural aggregates [34].

However, the problem associated with BOFS utilization as an aggregate in the concrete is the expansion of concrete [35]. Because the expansion of concrete is unacceptable according to the standard regulations, researchers are seeking ways of overcoming this issue. The process of f-CaO (free calcium oxide) and f-MgO (free magnesium oxide) hydration causes the concrete to expand. The hydration process of f-CaO and f-MgO develops high internal stress in the concrete matrix, causing the separate pores to merge into one common, and thus, a change in concrete volume occurs [36]. The f-CaO and f-MgO hydration process increases the volume of concrete by 91.7% to 119.6%, according to research by Wang et al. [37]. The expansion problems arise due to the formation of Portlandite ($Ca(OH)_2$) and brucite ($Mg(OH)_2$).

$$f\text{-}CaO + H_2O \rightarrow Ca(OH)_2 \quad (2.2)$$

$$f\text{-}MgO + H_2O \rightarrow Mg(OH)_2 \quad (2.3)$$

To overcome the soundness problem, steel slag is used in its fineness size. Thus, the hydration process is accelerated. Implication of steel slag rich in mineral composition, containing silicate, aluminum, and calcium, as admixture is advantageous for enhancing the mechanical and microstructural qualities of concrete [8]. Nonetheless, grinding the steel slag to the fine powder form is economically ineffective due to its toughness. A more practical, affordable, and assuring approach is to use BOFS as an aggregate [9]. As a result, the replacement of cement by BOFS is beneficial for by-product utilization and the development of concrete properties.

2.4. Geopolymers

Geopolymers or alkali aluminosilicate material is formed during chemical processes by using aluminosilicate sources and alkali-activated solutions [38]. Geopolymers can perform similarly to conventional cementitious binder materials in various uses but with the added benefit of a smaller environmental footprint by reducing greenhouse gas emissions [39]. The mechanical, chemical, durability, and microstructural properties of geopolymer are influenced by the raw materials used for its manufacture. Recent studies showed the outstanding performance of geopolymers in the construction materials sphere as a material that can be used for construction and repair works [40].

There are 4 main components of geopolymer: binder, alkali-activated solution, aggregate, and water. Industry-product materials might fully or partially replace the binder and aggregate material in the geopolymer mixture. Thus, geopolymer is considered to be environmentally friendly not only in terms of limiting greenhouse gas emissions but also in terms of utilizing industrial by-product materials.

2.4.1. Geopolymerization

The geopolymerization reaction occurring between aluminosilicate source and alkali activator was proposed in 1950 by Glukhovsky [41]. The geopolymerization reaction has four transformation reactions: destruction, coagulation, condensation, and crystallization. These transformation reactions occur in three stages: In the first stage, the alkali activator solution dissolves the aluminosilicate source by destroying the bonding of the aluminosilicate source and by forming free silica and alumina tetrahedron units. Then, the shift of the alkali activator from the liquid to the gel phase indicates the coagulation process [42]. In the second stage, the condensation process occurs under the hydrolysis reaction, where the water is evaporated from alumina and silica hydroxyl by forming the gel phase. Furthermore, the crystallization process is initiated under the gel hardening action. As a result, the three-dimensional aluminosilicate amorphous structure is formed, which composes the constituent of the geopolymer.

In the geopolymerization process, an alkali activator solution is assigned a crucial role. The greater molarity of NaOH impacts a larger disintegration rate of the silica and alumina ions from the aluminosilicate sources [43]. Consequently, a faster dissolution rate results in a faster geopolymerization reaction. In addition to the elevated molarity of NaOH, Zhang et al. [44] state that the reaction temperature affects the rate of geopolymerization. Thus, higher temperatures result in faster geopolymerization, which can be proved by the appearance of amorphous peaks in the XRD pattern. The geopolymerization process is beneficial in inhibiting the expansion problem related to BOFS.

2.4.2. Source materials

Many academics find that a wide range of industrial by-products are interesting research topics on the basis of identifying suitable waste material for geopolymer manufacture. The primary determinants in choosing the source material are the industrial by-products' physical characteristics, cost, and abundance. An industrial by-product comprising silicon (Si) and aluminum (Al) in non-crystalline state can be chosen as a possible source

material for geopolymer. A vast amount of research was conducted on using different by-product materials as source materials of geopolymer, such as metakaolin, fly ash (FA), ground granulated blast furnace slag (GGBFS), and rice husk ash.

According to Davidovits [38], the geopolymer mixtures with calcined substances such as steel slag and FA yielded substantially greater compressive strengths than those formed from non-calcined minerals like metakaolin clay. Nevertheless, metakaolin is demanded due to its prominent ability to dissolve in the alkali activator solution and monitor the Si to Al ratio and its white color [45]. However, due to the high price of metakaolin, its utilization in large-scale production of concrete is restricted.

Barbosa and MacKenzie [46] discovered that the source material that underwent calcination yielded a greater value for compressive strength when compared to the non-calcinated source material. Nonetheless, the reaction time and compressive strength value were better when the source material was a combination of calcined and non-calcined [47].

The most suitable properties of FA as a binder are observed for FA, which is comprised of a low calcium content. Van Jaarsveld et al. [48] investigated high-calcium FA-based geopolymer and discovered that high-calcium FA is the cause of high compressive strength development, which is the result of calcium compounds forming at an early age.

Fly ash (FA)

One of the by-products of burning coal is FA. The variety of coal ignited determines the FA's characteristics and chemical makeup. FA is primarily composed of silicon oxide (SiO_2), aluminum oxide (AlO_3), and iron oxide (FeO_3). There are two types of FA: Class C and Class F FAs. Class C FA has a high CaO content exceeding 20% of the total weight, while Class F FA has a low CaO content that does not exceed 10% by weight [49]. FA particles are smaller than OPC particles in terms of size. It varies from 1 μm to 150 μm [50]. Fine particles of FA are beneficial for production of geopolymer due to their high reaction rate and ability to fill the voids, leading to a stronger and denser structure. The rounded particles of FA improve the geopolymer's workability [51].

Ground granulated blast furnace slag (GGBFS)

A by-product of the iron industry is ground granulated blast furnace slag (GGBFS). Iron ore, limestone, and coke are supplied into a furnace and heated to 1500°C during the production of iron. The final product of the furnace is a liquid iron and slag at the top. In order to obtain GGBFS from slag, it is immersed in water to develop cementitious properties, and after solidification, it is grounded into fine particles [52]. Calcium oxide (CaO), SiO_3, and

Al_2O_3 comprise the main chemical constituition of GGBFS. Other metal oxides can be found in the composition of GGBFS.

According to researchers, GGBFS, as part of the FA-based geopolymer, increases compressive strength, decreases flowability, and speeds up the setting time of the geopolymer [53]. While FA-based geopolymer requires curing at high temperatures to obtain specific properties, incorporating GGBFS can lower the required curing temperature. However, the incorporation of GGBFS should be limited to a specific amount, as it might lead to the brittleness of the geopolymer. According to Deventer et al. [54], geopolymers made with GGBFS are resilient to fire exposure, sulfate attack, water permeability, acid attack, and corrosion. The formation of calcium silicate hydrate (C-S-H) gels and aluminosilicate hydrate (C-A-S-H) gels during the hydration and polymerization processes favors the development of the properties of geopolymer, as mentioned above [55].

Alkali activator.

Alkali activator is a crucial part of the production process of geopolymers because it starts the geopolymerization reaction. There are three common alkali activators which are used in geopolymer mixtures: NaOH (sodium hydroxide), Na_2SiO_3 (sodium silicate), and KOH (potassium hydroxide). The alkali activators can be used in combination or alone. Since Na_2SiO_3 is the most widely utilized alkaline activator mixed with NaOH, Na_2SiO_3 to NaOH ratio affects the geopolymer's mechanical properties. Development of mechanical properties is more apparent at Na_2SiO_3/NaOH ratio between 0.4 and 2.5 [56].

NaOH is usually produced in a solid state (flakes or pellets), which is required to be converted into a solution. The NaOH pellets should be attenuated in the aqua to obtain the specific NaOH solution concentration, referred to in moles (M). 400 grams of NaOH flakes should be attenuated in 1 liter of water to obtain a 10M NaOH solution. NaOH concentration plays an important role in the improvement of geopolymer strength, and the optimal concentration is in the range of 8M to 16M. Since NaOH molarity and the ratio of Na_2SiO_3/NaOH have an impact on the geopolymer's workability and setting time, the lowering of ratio and molarity increases the flowability and shortens the geopolymer's setting time [57]. According to Malkawi et al. [57], the geopolymer's initial characteristics (workability, setting time) are primarily affected by NaOH, while the strength and microstructural properties obtained after some periods of time depend on Na_2SiO_3.

According to Jegan et al. [58], sodium-based activators are more preferred in terms of developing the geopolymer's compressive strength than potassium-based activators.

Aggregate

A frequently used fine aggregate in OPC concrete is natural river sand. Sand, in combination with coarse aggregate, gives a desired property to the concrete [59]. Because the aggregate type used in manufacturing geopolymer influences its strength, it is crucial to utilize aggregate of exceptional quality. According to Lohani et al. [60], the exploitation of sand as an aggregate is restricted for two reasons: a deficit of sand in some regions and continuous extraction of sand from rivers have an adverse effect on the surroundings. Therefore, the demand for alternative aggregate is increasing because of the increase in construction.

Various research has been conducted on using slag and glass as a substitute aggregate source in concrete production. Glass utilization as an aggregate has a favorable effect on the environment, as its degradation in the landfill requires a million years [61]. According to Adaway and Wang [62], replacing sand with glass sand by 30% in the OPC concrete composition improves its compressive strength.

Steel slag aggregate (SSA) is a promising type of aggregate in the building sector due to its encouraging physical and durability characteristics [63]. Several treatment processes, such as carbonization and weathering, are applied to the SSA to prevent its expansion in the structure [64]. The formation of stable carbonate and hydroxide during the treatment proved to be an efficient method of treatment. However, the high cost and required equipment are the main obstacles to applying these treatments.

2.4.3. Mixture proportions

The mixture proportions of the geopolymer affect its initial and final properties. According to Brough and Atkinson [65], it is difficult to identify which components of geopolymer have significantly affected their specific properties, but all elements have an impact on the geopolymer's properties. Thus, several research studies have been carried out to study the effect of mixture parameter variation on the properties of geopolymers. The binder's strength is primarily determined by the amount of GGBFS content [48]. Thus, increasing the GGBFS to FA ratio increases the compression strength of the geopolymer. Nevertheless, the high content of GGBFS lowers the geopolymer's workability. According to Koushkbaghi et al. [66], the high content of FA as a binder material reduces the segregation and bleeding of geopolymer. Long et al. [67] studied 7 different GGBFS to FA ratios (1:1, 0;5, 1;4, 2:3, 3:2, 4:1, and 5:0) to identify their effect on geopolymer compression ability and microstructural characteristics. GGBFS to FA ratio 1:1 samples have no discernible improvement in

compressive strength with time. The geopolymer blends with fly ash as the sole binder material demonstrated the least compressive strength. The mixture containing only GGBFS as a binder material experienced a reduction in the strength of compression over time. The geopolymer mixtures containing both FA and GGBFS revealed an increase in the strength of compression throughout the curing time. An rise of the GGBFS/FA ratio yielded enhanced compressive strength. Thus, the optimum ratio is 4:1. However, a high ratio of GGBFS/FA resulted in the formation of brittle crystalline phases, leading to the destruction of dense structure of the geopolymer. As a result, the geopolymer samples' compressive strength decreases with time.

The alkali-activator solution (AAS) to binder ratio is also one of the significant mixture design parameters influencing the geopolymer concrete's mechanical characteristics. According to the experimental endeavors conducted by Morsy et al. [68], the ascend of AAS to binder ratio to 0.400 from 0.325 and 0.475 from 0.325 increased the flowability of the geopolymer by 14% and 21%, respectively. When the AAS/binder ratio increases, there is a discernible decrease in compressive strength, which occurs due to the higher permeability and porosity of the concrete. Thus, the AAS/binder ratio of 0.400 is the optimal value under which the development of flowability compensates for the negligible decrease in compressive strength.

The rise of NaOH concentration significantly affects the fresh and hardened characteristics of the geopolymer. As the concentration of NaOH rises, the compressive strength of the geopolymer increases and its flowability decreases. According to Aliabdo et al. [69], the flow rate of the concrete decreases due to an enhanced geopolymerization reaction, which takes into account NaOH's high molarity. High molarity of NaOH leads to denser structure formation, enhanced microstructure, and early strength development.

Morsy et al. [68] states that increasing the Na_2SiO_3/NaOH ratio from 2 to 2.5 improved the compressive strength and from 2.5 to 3 adversely affected the flowability and compressive strength of the geopolymer samples. Slump loss results from the viscous nature of sodium silicate. One of the key mixture characteristics of geopolymer that affects its mechanical and fresh properties in the geopolymer mixture is the water to binder ratio (w/b). According to research on the effect of w/b ratio variation, the optimal w/b ratio falls between 0.25 and 0.35. It is found that increasing the w/b ratio increases the flowability and decreases the compressive strength of the geopolymer [70]. Adam [71] reported a similar research output, with the indication that the optimum w/b ratio was 0.32.

2.5. Curing Regimes

2.5.1. Steam curing

Steam curing is a vapor curing method under atmospheric pressure conditions. In nature, the hydration process occurring in the concrete is accelerated since steam curing is a type of curing where much moisture is produced. As a result, early-age concrete strength development takes place. Steam curing is usually carried out at a temperature from 40 to 100°C. Higher temperatures and longer curing times increase the hydration rate of cement in concrete [72]. Nevertheless, research has shown that the production of ettringite during steam curing at temperatures higher than 80°C has a detrimental effect on the microstructural characteristics of concrete.

In contrast to samples that are cured at a higher temperature and for a shorter time, Zeyad et al. [72] states that steam curing at a lower temperature in the range of 45 to 60°C and a longer curing time of 24 hours produces both high compressive strength at later ages and high early-age strength. Following the geopolymer concrete's casting, Lloyd and Rangan [73] examined how the rest period affected the concrete's mechanical properties. As a result, it was found that the samples that were steam-cured after a 24-hour rest period obtained higher compressive strength than samples that were immediately steam-cured after casting.

The study by Zheng et al. [74] compares curing methods: standard, steam, and autoclave. It was discovered that the steam curing method yields the highest development of compressive strength. Steam curing took place for two, four, and eight hours at 80°C. Higher compressive strength was obtained with a longer curing period. Similar research was carried out by Yewale et al. [75], in which the effect of steam curing and water curing on the development of mechanical properties of geopolymer was studied. It was established that the compressive strength of concrete improves at higher temperatures, and the optimum temperature was found to be 80°C. Compared to steam-cured samples, the water-cured samples exhibited relatively low compressive strength after 28 days of testing, which shows that low temperature leads to low strength development.

The impact of steam curing on the drying shrinkage of geopolymer demonstrated that the primary cause of shrinkage is the creation of negative pressure in the capillary framework of the geopolymer [76]. Nevertheless, the drying shrinkage rate for steam-cured samples is relatively low compared to the samples that are ambient air-cured. The condensation process in geopolymer samples, which is associated with the moisture loss from capillaries, is

accelerated by steam curing. Thus, significant drying shrinkage occurs at the initial stage of curing, and further on, it is stabilized.

2.5.2. Ambient air curing

One kind of curing done at room temperature and relative humidity is called ambient air-curing. The specimens cured at ambient temperature possess smaller early-age strength in comparison to samples cured elevated temperatures due to the slow rate of geopolymerization. Nath and Sarker [77] reported that slag incorporation shortens the setting time and boosts the compressive strength of FA-based geopolymer that has been cured at ambient temperature. Moreover, compression strength decreases, and setting time increases with increasing alkali activator content. Slag incorporation and a reduction in the alkali activator are beneficial to the geopolymer's properties in ambient air-cured conditions. Nath et al. [78] researched the impact of adding fly ash and slag on geopolymer's early strength and workability development in 2014. The obtained values were discovered to be comparable to the OPC concrete values. Furthermore, they discovered that because of its early strength development and internal heat generation, GGBS aided the ambient air-curing process.

Vijai et al. [79] experimented with geopolymer samples to examine the differences in mechanical properties between ambient air and heat curing. The heat-cured samples had compressive strength values that were 7 and 2 times higher than those of the ambient air-cured samples, respectively, according to the 7-day and 28-day compressive strength tests. On the other hand, compared to heat-cured samples, ambient air-cured samples exhibit a more remarkable development of strength. As a result, for both heat- and ambient air-cured samples, the 28-day compressive strength values increased by 4.5 and 1.2 times, respectively, compared to the 7-day test values. A similar conclusion was made by Nurruddin et al. [80]: with increasing curing age, concrete subjected to ambient air-curing develops its compressive strength, while the samples exposed to oven curing show negligible changes in compressive strength with age of curing.

Temuujin et al. [81] states that research has been done on the impact of fly ash milling on the ambient air-cured geopolymer's mechanical characteristics. Due to the higher reactivity of the finer fly ash particles, it is discovered that they contribute to a higher strength development at room temperature. Research was done by Chouksey et al. [82] to compare the effects of ambient air-curing and oven-curing techniques on geopolymer concrete's mechanical and microstructural characteristics. Air-cured specimens have a higher density and drying shrinkage than oven-cured specimens. Due to the slow geopolymerization

reaction, a large amount of water evaporation from the geopolymer structure accounts for the higher drying shrinkage in air-cured specimens. Since the geopolymerization process is accelerated in oven-cured specimens, the water in capillaries is retained, leading to slower evaporation. XRD results showed that the content of oxide minerals in oven-cured samples has a lower peak than that of ambient air-cured samples, which indicates the complete geopolymerization reaction. Regarding the microstructural properties obtained from the SEM image, it is found that the ambient air-cured sample leads to the creation of an interior structure that is less porous and more homogenous. In contrast, the elevated temperature might be the reason for pores and honeycomb formation [82].

2.5.3. Water curing

Water curing is widely used for concrete curing to improve its mechanical and microstructural properties. Water curing is carried out by following the ASTM C511 [83] standard specification. The water curing procedure involves immersing the concrete samples into water at room temperature; the storage tank should be made from non-corrosive material. Lime should be added to the potable water to prevent the washout of calcium hydroxide from the concrete samples [83].

The strength of the concrete continuously rises while it is being cured and stops rising after the curing process is completed. Since the hydration of the cement practically requires moisture, adequate humidity levels are essential. According to Neville [84], the hydration process stops when the concrete capillaries' relative humidity is 80% or lower [84]. Shortage of required water leads to insufficient development of concrete properties, such as strength and impermeability [85]. Apart from mechanical issues, there is also a risk of durability issues related to the appearance of micro-cracks and drying shrinkage.

Termkhajorknit et al. [86] conducted experimental work to study the effect of water curing on different fly ash and cement contents in FA-cement-based paste. Overall, water-cured samples containing 100% cement have a higher compressive strength than samples containing FA. Additionally, 7-day and 3-day water curing resulted in lower compressive strength values over all ages of samples compared to samples continuously cured in water. The strength value increases with age and is more apparent for the FA samples. Because samples containing 25% FA are not affected by water curing duration, the compressive strength values are relatively similar for each specific age of concrete. Continuous water curing is favorable for samples containing 50% FA compared to water curing of 3-days and 7-

days. Until the sample's age of 50 days, the compressive strength values are relatively similar, but the strength value of continuously water-cured samples shows an explicit increase.

According to Termkhajornkit et al. [86], the hydration process of FA in the mixtures with 25% FA and 50% FA is steady for the first 91 days, but the further hydration process of FA sharply increases. Continuous water curing compared to 7-day water curing shows a higher degree of FA hydration. It is noteworthy that even after water curing completion (7 days), the hydration process of FA can be observed at an increasing rate. This might be explained by the pozzolanic reaction initiated by residual water in the sample capillaries.

Vazinram et al. [87] compared the effect of water curing and lime water curing regimes on the mechanical properties of the OPC concrete with the partial substitution by pozzolan material (ZnO_2). The presence of $Ca(OH)_2$ in the limewater enhances the creation of C-S-H gel by reaction with pozzolan material, improving concrete strength. Furthermore, the development of C-S-H gel facilitated the decrease in the concrete structure's water permeability. Bediako et al. [88] conducted similar research comparing concrete and mortar samples' water and lime water curing. It is found that limewater curing prevents the calcium hydroxide leaching process from concrete, leading to less C-S-H gel in the concrete structure. Subsequently, it leads to poor compressive strength development.

2.5.4. Carbonation/Mineral Sequestration

Carbonation curing is a relatively new method, presumably decreasing the CO_2 footprint in the environment during concrete production. The carbonation is carried out in a special storage tank under specific temperature, humidity, and CO_2 concentration. The effect of CO_2 curing can vary widely depending on these factors.

Sandybay et al. [89] investigated the impact of CO_2 curing time on the permeability, compressive strength, and tensile strength of previous geopolymer concrete (PGC). Expanding the carbonation time causes the samples' early-age compressive and tensile strengths to decrease and their permeability to increase. The study conducted by Harirchi and Yang [90] yielded controversial results regarding the effects of carbonation curing duration on the properties of FA-based geopolymer. Compared to samples without carbonation, the compressive strength of geopolymer is significantly impacted by carbonation curing on the first day of curing. However, among the CO_2 cured samples, the highest compressive strength is obtained for samples cured for 24 hours and 3 days compared to 3, 6, and 12 hours cured samples. Such a pattern is explained by the formation of calcium carbonate from calcium silicate's reaction with CO_2 and their absorption after 12 hours of CO_2 curing.

The study conducted by Huang et al. [91] on the effect of carbonization on the performance of OPC and geopolymer concrete is shown in Figure 2.1. Two types of samples were carbonized in the carbonation chamber for 3, 7, 14, and 28 days. The established test conditions included 20% CO_2 concentration, 70% relative humidity (RH), and a temperature of 20℃. According to the obtained data, the carbonization process mostly affected the OPC concrete (PCC). Thus, an increase of compressive strength from 48.9 to 63.7 MPa is observed, and the highest rise of compressive strength occurred during the 7-day carbonization process. While the compressive strength of FA-based geopolymer concrete (FGC) experienced a decrease during the first day of carbonization, the rapid growth of strength was observed at a later age. It is observed that concrete lost ductility and became more brittle due to carbonization, despite the fact that this also impacted PCC's compressive strength. However, the carbonization process had minimal effect on the geopolymer concrete [91].

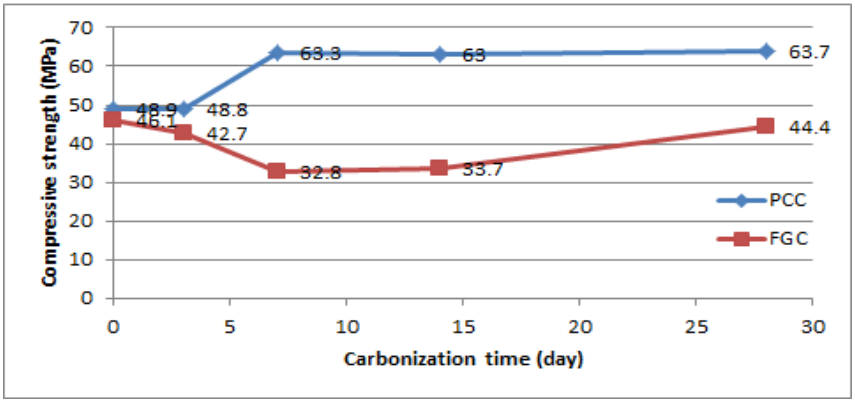

Figure 2.1: The effect of carbonization time on compressive strength

Note. Reproduced from [91, Fig. 2]

Beltrame et al. [92] obtained the similar results to Huang et al. [91], where the carbonation effect on geopolymer and OPC concrete are studied. The experimental work was studied by curing samples at 50℃ temperature for 24 hours. Then, carbonation curing was carried out for 6 hours, at a CO_2 concentration of 99%, 25±5 ^{o}C temperature, and ambient RH, referred to as step 2. Step 3 in this experimental work is ambient air-curing. Overall, 2 types of concrete are compared: geopolymer and OPC. These samples are carbonated (C) and non-carbonated (N). As presented in Figure 2.2, compared to OPC concrete, geopolymer concrete has a higher compressive strength. However, compressive strength development with time is more evident for carbonated OPC concrete. As Beltrame et al. [92] explains, because CO_2

uptake for OPC concrete is higher than for geopolymer concrete, the strength development would be more apparent for C-OPC concrete.

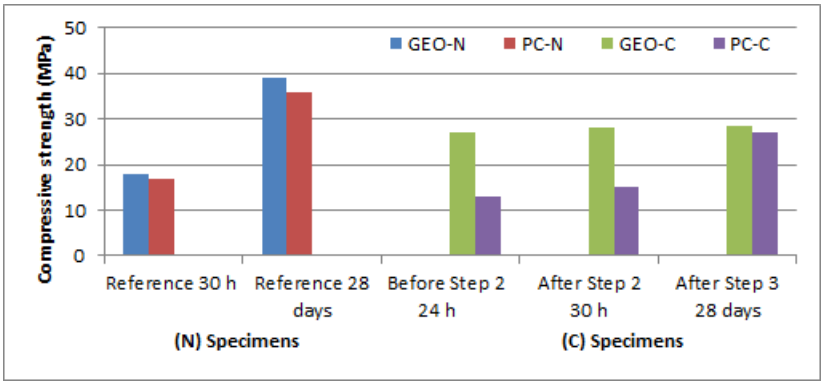

Figure 2.2: Comparison of compressive strength value at different ages

Note. Reproduced from [92, Fig. 5]

2.6. Properties of BOFS-based geopolymer

Compressive strength

The GGBS/FA ratio and the SiO_2/NaO ratio were discovered to affect the mortar's compressive strength. With an increase in the SiO2/NaO ratio, geopolymer mortar's compressive strength rose. As a result, at 56 days, the samples with 1.28 and 1.6 SiO_3/Na_2O ratios had compressive strengths of 32 and 53 MPa, respectively. When f-CaO and f-MgO come into contact with SiO_2, which produces stable silicate compounds, is the cause of the developed compressive strength [6]. According to Lee et al. [6], increasing the quantity of GGBFS improved the strength in compression of the mortar. The GGBFS highly affects The arrangement of the mortar by making it denser. It was discovered, nevertheless, that depending on the quantities of BOFS, the molarity of NaOH had a distinct impact on the compressive strength of geopolymer paste. It was found that thea rise in the molarity of NaOH at 3 and 7 days improved the compressive strength value of the geopolymer paste that contained 0% and 20% BOFS. Nevertheless, the high molarity of NaOH solution significantly decreased the geopolymer paste's compressive strength at 28 and 90 days of age. As the molarity of NaOH increased, the compressive strength of geopolymer samples containing 40% BOFS dropped. The most pertinent molarity for effectively developing compressive strength at 3 and 7 days is between 8 and 10 M NaOH. Nevertheless, the increase in molarity for samples containing more than 40% of BOFS resulted in strength reduction.

In order to determine how alkali activator type and aggregate affected the characteristics of the metakaolin-based geopolymer, Sun et al. [9] carried out an experiment.

Using BOFS as an aggregate resulted in higher compressive strength than limestone aggregate. Sodium Silicate, in combination with BOFS, is proven to be a better alkali activator. According to Sun et al. [9], BOFS aided in the development of ITZ and hardness in geopolymer concrete. During the geopolymerization process, BOFS hydrates to form C-A-S-H gel.

BOFS utilization as an aggregate material combined with river sand in geopolymer shows an increase in compressive strength from 7 to 28 days. Further, from 28-day to 56-day age, a reduction in compressive strength is observed [93]. Large amounts of silicon and aluminum in the geopolymer raw material support the increase in compressive strength up to 28 days of age. However, the reduction of the components mentioned above in the geopolymer structure ceases the further increase of compressive strength. Kareken et al. [93] came to a similar conclusion as Sun et al. [9], that the C-A-S-H gel developed from the hydration of BOFS, in combination with N-A-S-H, results in the development of geopolymer compressive strength.

The dissolution and dispersion of geopolymer components like silicon and aluminum as well as the creation of N-A-S-H gel are more explicit at a higher temperature (80℃) rather than at a lower temperature (20℃). However, a further temperature rise could have a negative impact on compressive strength development. Falayi [94] examined the impact of three different curing temperatures, 50, 70, and 90°C, on the geopolymer continuing BOFS compressive strength. It is discovered that the creation of C-A-S-H gel is impacted by the delayed dissolution of CaO at 90°C.

Scanning electron microscope (SEM) image

SEM analysis is a testing procedure where the internal microstructure of the samples is investigated in terms of the presence of microcracks, pores, and unreacted particles. Falayi [94] investigated and compared the microstructure of FA-based geopolymer with BOFS-based geopolymer. In comparison to FA-based geopolymer, the BOF-based geopolymer has more geopolymer gel (C-A-S-H) in the structure, while the former consists of unreacted particles. Additionally, it is clear from SEM images that the connection between particles in FA-based geopolymers is poor, and the connection between BOFS-based geopolymer particles is dense.

The SEM image comparison of limestone aggregate and BOFS aggregate in the geopolymer matrix revealed that utilization of BOFS as an aggregate result in denser structure and less obvious transition of aggregate to gel phase, compared to limestone [9]. Strong

bonding between aggregate and binder is the primary cause of the elevated compressive strength of geopolymer samples containing BOFS as an aggregate. According to SEM-EDS, the dispersion of Ca is more centered on the aggregate part, while Na is more centered on the gel part of the limestone geopolymer. The reason for such patterns is that Ca is the major component of limestone, while the amount of Ca in the metakaolin (binder) is low. In the case of BOFS geopolymer, the dispersion of Ca and Na is uniform, which shows that the Ca releases from aggregate and diffuses in all parts of the geopolymer [95]. The sodium aluminosilicate hydrate (N-A-S-H) gel formed in the binder system in combination with C-A-S-H gel is reported to bind the adjacent solid/aggregate particles by creating the dense Interfacial transition zone (ITZ). Consequently, it results in a decrease of the porosity within the geopolymer structure. The rough texture and asymmetrical shape of BOFS aggregate enhance the interparticle bonding.

According to Mareya et al. [96], the higher NaOH concentration resulted in a faster and more intense geopolymerization reaction, which is apparent from SEM-EDX images. The 2 M NaOH and 8M NaOH are compared according to SEM images. The samples with 8M NaOH are more homogeneous in structure, while the sample with 2M NaOH has unreacted particles present in the matrix structure. Additionally, EDX analysis revealed numerous and more intense peaks of Ca and Si in 8M NaOH geopolymer samples. Mareya et al. [96] also studied the effect of curing temperature on the microstructure of geopolymer samples. During the 60 ℃ curing, it is revealed that the geopolymerization reaction is not completed, and some unreacted particles can be observed in the structure of the geopolymer. According to Mashifana et al. [97], geopolymer gel formation is slow under low curing temperatures. The sample cured at 90 ℃ shows the dense and uniformly packed geopolymer structure compared to the sample cured at 60 ℃. However, due to the fast geopolymerization process and accelerated hardening, micro-cracks formation becomes an issue for samples cured at elevated temperatures.

Fourier Transform Infrared Spectroscopy (FTIR)

The substitution of BOFS with rice husk ash (RSA) in geopolymer revealed that the peaks shift to the lower wavenumbers [96]. The shift of wavenumber can be correlated to compressive strength. When the RSA replacement factor increases, the wavenumber decreases, and the compressive strength also decreases. According to Mareya et al. [96], such a pattern is observed because of an intensive reaction between RSA and sodium hydroxide, leading to an incomplete geopolymerization reaction due to insufficient NaOH. NaOH

concentration increase revealed the formation of a broad peak between 2945 and 3710 cm^{-1} wavenumber and the shift of other peaks to higher wavenumber frequencies.

Mashifana et al. [97] states that the broad peak between 2945 and 3710 cm^{-1} represents the hydroxyl group's stretching and deformation. Apparently, water is trapped in the geopolymer system. The O-C-O bonding stretching vibration can be seen at the peak of 1384-1386 cm^{-1} induced by the carbonation process. In Mareya's et al. [96] experimental work, the process of carbonation took place because aqueous NaOH and CO_2 reactions from the atmosphere. The Si-O-Si symmetric bands are discovered at lower wavenumbers. The 618 cm^{-1} and 1637 cm^{-1} peaks reveal the absorption of binder materials and the formation of Si-O-Si and Si-O-Al symmetric vibration bands, respectively. At a higher curing temperature, the above-mentioned bands move to a greater wavenumber and get sharper, indicating the rapid alkali-silica reaction occurrence. The formation of alumino-silicate gel in the geopolymer matrix can be correlated to intense peak formation.

It is found that utilization of KOH leads to intense peak formation at a frequency of 2300 cm^{-1} [97]. NaOH and KOH-activated geopolymers' apparent peak at 1000 cm^{-1} indicates Si-O-Si bonds formation [98]. Several articles indicated the main band formation at a 1000 cm^{-1} wavenumber, which indicates the formation of tetrahedral structure of Al and Si from precursor materials.

The band shift to a lower wavenumber value of geopolymer in comparison to the original band in raw material indicates the geopolymerization reaction. Falayi's experimental work [94] showed that the geopolymer containing BOFS experienced a larger shift to the lower wavenumber value in comparison to the geopolymer containing FA. Thus, it indicates a higher geopolymerization reaction process and higher compressive strength.

X-ray diffraction (XRD)

X-ray diffraction analysis is conducted to identify the formation of new crystalline structures in the geopolymer matrix. Lee et al. [6] concluded that the geopolymer technique is suitable for stabilizing the BOFS. The stabilization of BOFS is attributed to the vast amount of silicon left unreacted in the geopolymer. According to Lee et al. [6], the crack appearance on the surface of BOFS facilitates the reaction mechanism between silicon and f-CaO and f-MgO. The formation of stable compounds such as calcium silicate and magnesium silicate inhibits the expansion problem of BOFS-based geopolymers.

The XRD analysis on geopolymer revealed the reduction of silicon peak compared to the precursor material, indicating its dissolution under an alkaline activator solution [94]. The

formation of new crystalline phases of C-A-S-H and C-S-H gel at peaks 25° and 30° testifies to the geopolymerization reaction [99]. The geopolymer gel N-A-S-H phase is also found in the geopolymer matrix. However, more BOFS contents result in more C-A-S-H and C-S-H phase formation.

Chapter 3 – Research methodology

3.1. Materials

3.1.1. Binders

The current work uses fly ash (FA) and ground granulated blast furnace slag (GGBFS) as binder materials. GGGBF is supplied by the "Mechel-Materials" laboratory in Chelyabinsk, Russia. The fineness of GGBF slag is 99.9%. According to the manufacturer, the summation of MgO, CaO, and SiO_2 in GGBFS content is about 78%.

The specific gravity of binders was determined according to ASTM C188-17 standard. The procedure for obtaining specific gravity values for binders is shown in Figure 3.1. First, binders (raw materials) such as GGBFS and FA are prepared. The pycnometer flask is thoroughly cleaned and filled with kerosene until the mark is between 0 and 1. Then, the pycnometer flask is weighed, and the value is recorded. The binder is slowly added into the pycnometer flask and periodically shaken. Finally, the weight and volume of the pycnometer containing kerosene and binder are recorded. Equation 3.1 shows the procedure of finding the density (ρ) of the binder by subtracting the mass (M_k) and volume (V_k) of kerosene from the mass (V_{k+b}) and volume (V_{k+b}) of kerosene and the binder and dividing it. Further, to find specific gravity, the density of the binder is divided by the density of the water (Eq. 3.2). Three trials (Table 3.1) were conducted to find the average specific gravity of 2.94 and 1.80 for GGBFS and FA, respectively.

$$\rho = \frac{M_{k+b} - M_k}{V_{k+b} - V_k} \tag{3.1}$$

$$Specific\ gravity(SG) = \frac{\rho_{binder}}{\rho_{water}} \tag{3.2}$$

Table 3. 1. Specific gravity values of binder materials

	Trial 1	Trial 2	Trial 3
GGBFS	2.96	2.91	2.94
FA	1.78	1.80	1.83

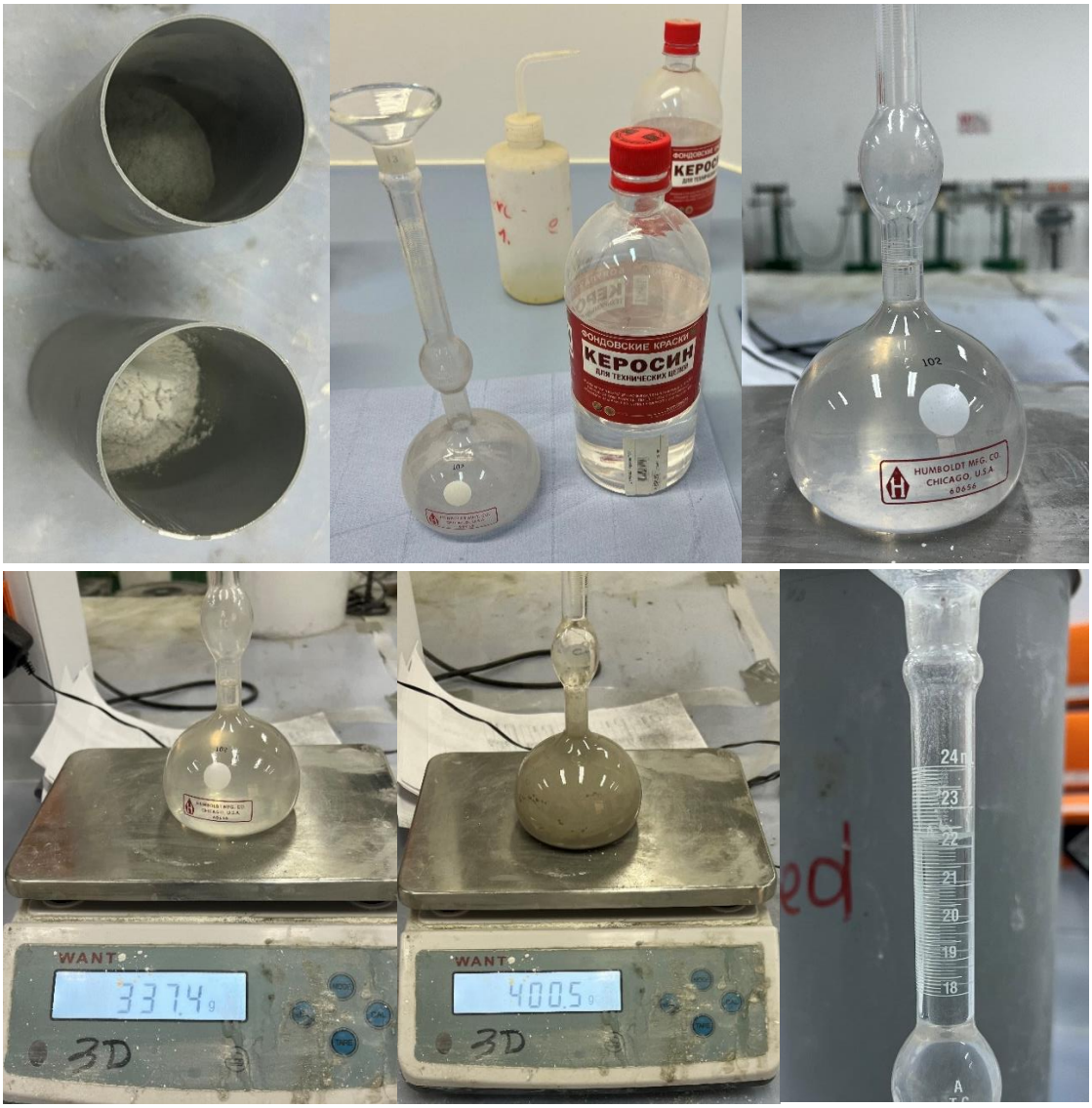

Figure 3.1: The procedure of determining SG of binder materials

The particle size distribution (PSD) analysis is carried out by using the Mastersizer 3000 equipment, shown in Figure 3.2. The PSD can be found using equipment that can measure particle sizes between 0.001 and 3.5 millimeters. The cumulative percent passing PSD is displayed in Figure 3.3. GGBFS is a fine material, where 100% of the particles passes through #325 (45µm) sieve size. While 73% of fly ash passes through #325 sieve size, the rest particle sizes exceed 45µm.

Figure 3.2: Mastersizer 3000

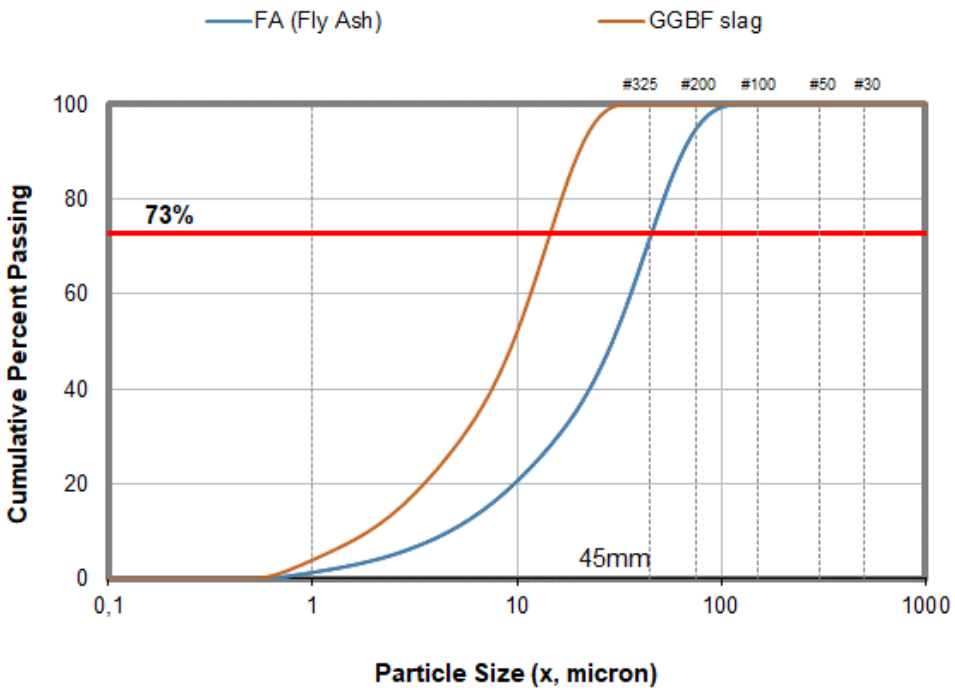

Figure 3.3: PSD of binder materials

The chemical composition of binder and aggregate materials was investigated using PANalytical Epsilon 4 equipment, shown in Figure 3.4. The equipment has the capacity to test 10 different materials simultaneously. Elemental and oxide composition of the materials can be found. The major chemical components of FA listed in Table 3.2 are SiO_2, Al_2O_3, and Fe_2O_3, which correspond to the chemical composition of FA found by Hardjito et al. [56]. GGBFS chemical composition is rich in CaO, SiO_2, and Al_2O_3.

The crystalline phases in FA and GGBFS are shown in Figures 3.5 and 3.6. The vast amount of mullite and quartz is present in FA. Crystalline phases of calcium compounds such as akermanite, calcite, and calcium silicate can be found in GGBFS composition, which corresponds to its chemical composition.

Figure 3.4: XRF equipment

Table 3. 2. Chemical Composition of FA and GGBFS

Chemical Composition	FA	GGBFS
SiO_2	62.15	23.97
Al_2O_3	20.39	5.9
Fe_2O_3	10.53	0.88
TiO_2	-	2.74
CaO	3.72	57.99
MgO	0.1	3.75
Na_2O	-	-
K_2O	1.31	1.12
P_2O_5	0.99	-
SO_3	0.24	2.47

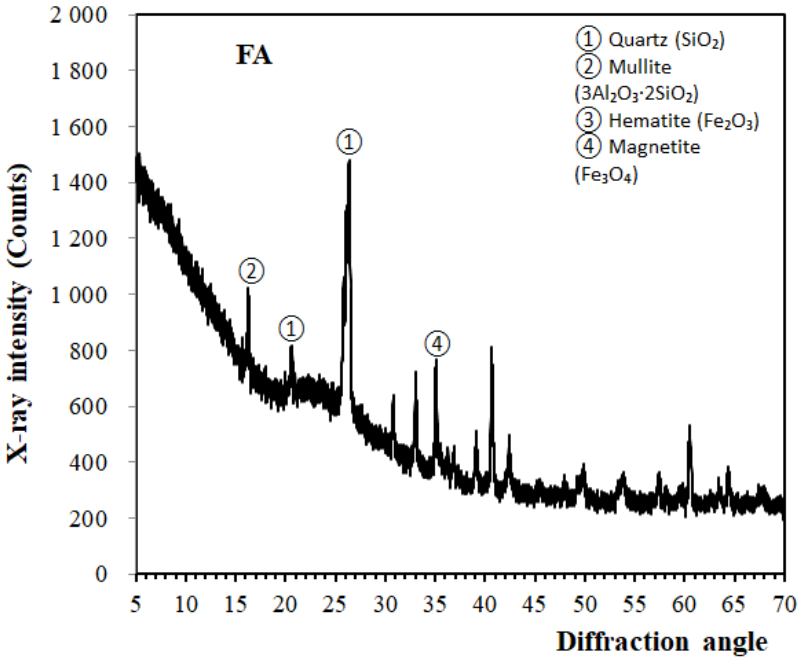

Figure 3.5: Crystalline phases of FA

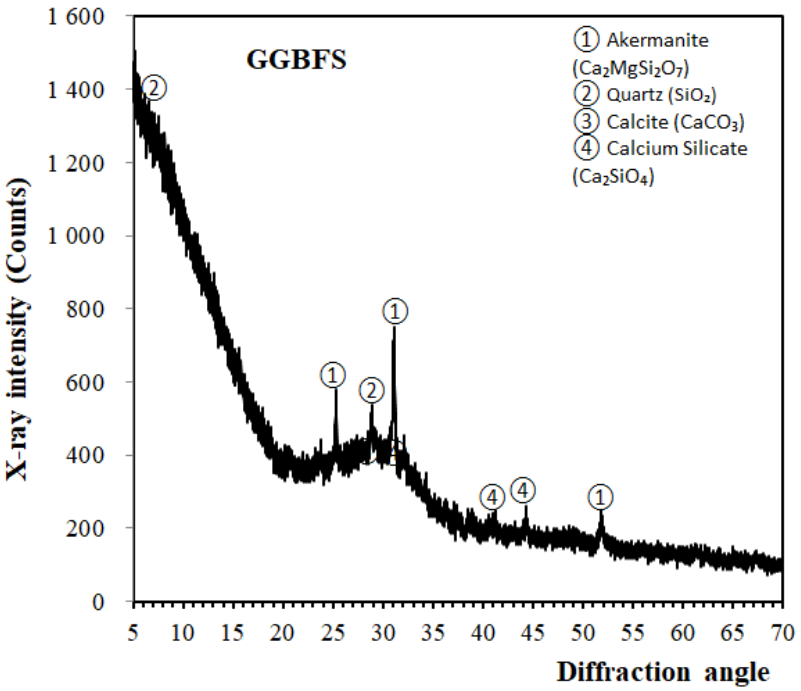

Figure 3.6: Crystalline phases of GGBFS

3.1.2. Aggregates

In this work, aggregates consist of a distinct blend of river sand and basic oxygen furnace slag (BOFS). The source of BOFS is the Temirtau region. Both BOFS and sand are dried in the oven for 24 hours at 95 ˚C and then sieved in the sieving machine. Required

particle sizes are defined by ASTM C1260 standard. Table 3.3 shows the required percentage of each sieve size per total aggregate mass.

Table 3. 3. Grading Requirement

Passing, sieve #	Retained, sieve #	Weight, %
4	8	10
8	16	25
16	30	25
30	50	25
50	100	15

Specific gravity (SG) and Absorption capacity (AC) are determined according to ASTM C128-15 to determine the further behavior of aggregates in the geopolymer mixture. Aggregates were first oven dried and sieved according to ASTM C1260 grading requirements for the trial tests to determine SG and AC. Then, dry aggregates are placed in zip pockets and moisturized with water. In order to obtain saturated surface dry (SSD) condition, aggregates are blow-dried. The sand cone shown in Figure 3.7 is used to check the SSD condition. It is filled with the aggregate in 3 layers by taping each layer 25 times. After removing the cone, the aggregate should crumble, but save the foundation. Aggregate in SSD condition is collected in the bowl and weighted. $Wt_{pyc+water}$ is obtained by weighting the pycnometer filled with the water to the top. Next, aggregate in SSD condition is placed in the pycnometer, filled with water, and then weighted ($Wt_{pyc+water+SDD}$). The system runs for 10 minutes after the excess water is carefully disposed of with no aggregate loss. Then, the remaining aggregate is oven-dried for 24 hours and weighted (Wt_{OD}). For both BOFS and sand, three trials (Table 3.4) were conducted to find the SG and AC, and the average values of SG were 2.7 and 3.3 for BOF and River Sand, respectively. The absorption capacity of BOFS aggregate is 8.91%, while that of river sand is 1.84%.

$$Apparent\ specific\ gravity(SG_a) = \frac{Wt_{OD}}{\left(Wt_{pyc+water} + Wt_{OD} - Wt_{pyc+water+SSD}\right)} \tag{3.3}$$

$$Absorption\ capacity\left(AC\right) = \frac{\left(Wt_{SSD} - Wt_{OD}\right)}{Wt_{OD}} \times 100 \tag{3.4}$$

Table 3. 4. Specific gravity and absorption capacity values of aggregate materials

	Set 1	Set 2	Set 3
BOFS (SG)	3.34	3.29	3.31
BOFS (AC)	1.78	1.86	1.86
Sand (SG)	2.71	2.77	2.67
Sand (AC)	1.90	1.86	1.77

Figure 3.7: Procedure of determining SG and AC of aggregate materials

The examination of the chemical makeup of sand and BOFS revealed the high content of CaO, Fe_2O_3, and SiO_2, as shown in Table 3.5. This corresponds to XRD analysis findings, where the high content of lime, hematite, and quartz in crystalline phases is present in BOFS aggregate structure, and the high content of quartz, hematite, and aluminum oxide in crystalline phases is present in sand, shown in Figures 3.8 and 3.9.

Table 3. 5. Chemical Composition of BOFS and Sand

Chemical Composition	BOFS	Sand
CaO	52.38	16.27
Fe_2O_3	29.39	13.81
SiO_2	7.39	54.51
MnO	4.33	1.51
MgO	3.13	0.78
Al_2O_3	1.53	5.71
SO_3	0.23	0.51
TiO_2	-	1.73
K_2O	-	3.65
P_2O_5	-	0.63

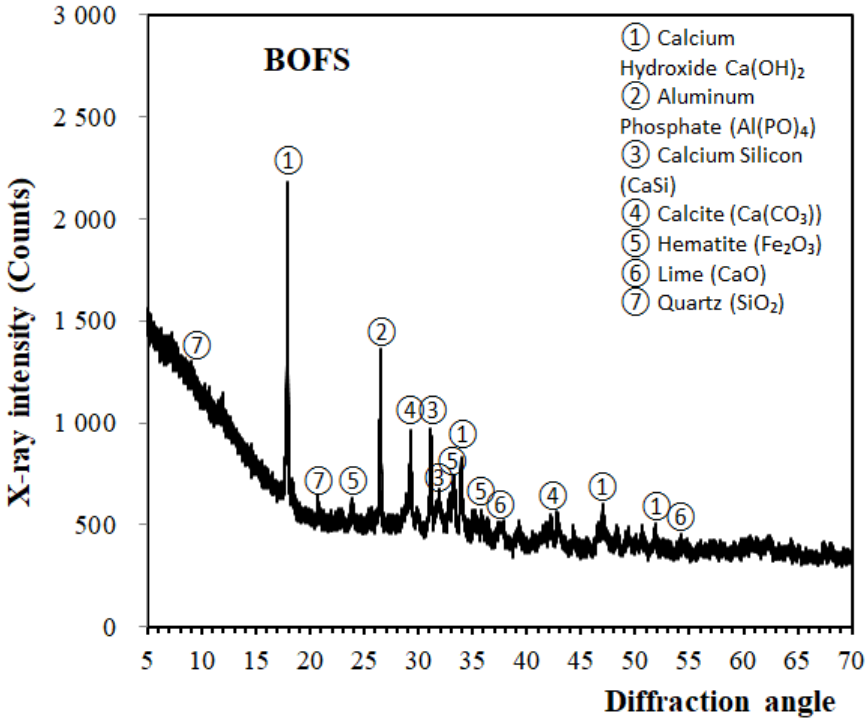

Figure 3.8: Crystalline phases of BOFS

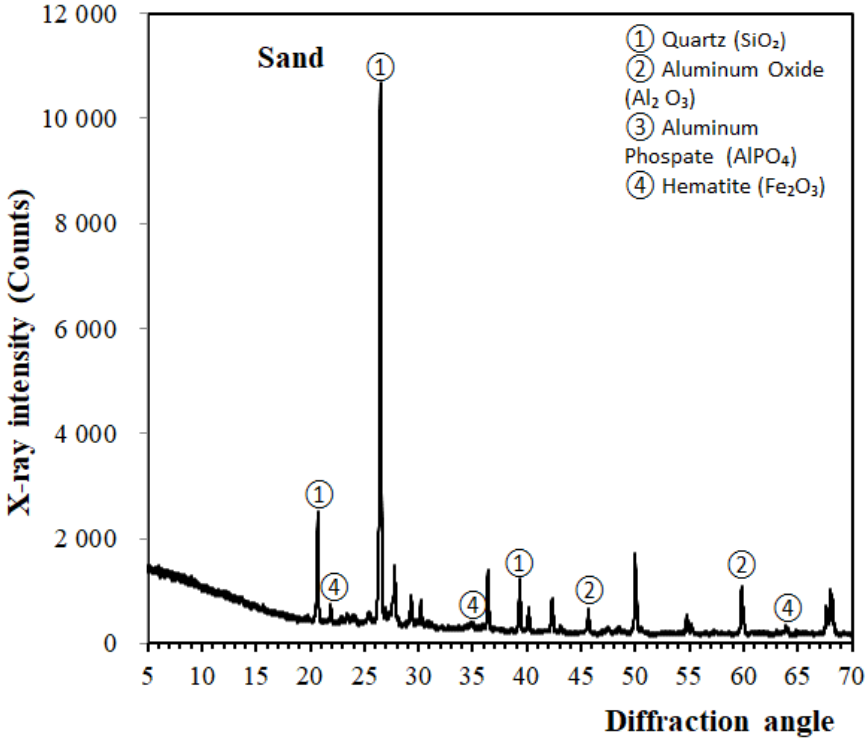

Figure 3.9: Crystalline phases of Sand

3.1.3. Alkaline Activators

The combination of sodium hydroxide (NaOH) and sodium silicate (Na_2SiO_3) is used as an alkali activator. Sodium silicate is supplied by the "Damu-Chemistry" company in Karaganda, Kazakhstan. The chemical composition of glass water is 28.7% of SiO_2, 10.23% of Na_2O, and 60.65% of water.

Sodium Hydroxide in the original pellet form is dispersed in water to produce 10 M of NaOH solution. The dissolution of 400 grams of NaOH pellets in 1000 grams of water yields a 10 M NaOH solution. The proportion is made based on the molecular weight of NaOH 40 g/mol. Sodium Silicate or water glass is already in solution form. The proportions of sodium hydroxide and sodium silicate are fixed at 1:2 for every mixture.

3.2. Mixture Proportions

In this research work, 15 mix designs are created to study the effect of the curing method and BOFS/sand ratio on the properties of geopolymer, as presented in Table 3.6. Alkali-activated solution (AAS) content and GGBFS/FA ratio are fixed variables 2 and 40/60, respectively. In most works, the steam curing is used to cure the geopolymer. Two steam curing durations are chosen, 6 and 12 hours, at the temperature of 80 ℃. Recent research indicates that prolonged steam curing at elevated temperatures is inadequate for the concrete's durability and compressive strength. After 12 hours of CO_2 curing, stable calcium carbonate is formed, so three mineral sequestration times 6, 12, and 24 hours were selected to investigate the effects on the geopolymer's mechanical and durability properties.

The high content of GGBFS decreases workability but increases compressive strength, according to Van Jaarsveld et al. [48], Koushkbaghi et al. [66], and Long et al. [67]. Thus, the optimum GGBFS to FA ratio is chosen to be 40/60. According to Morsy et al. [68], the optimum AAS content is 2, as further increases cause a loss of flowability, while decreases result in a decrease of compression strength. The water to binder ratio of 0.32 and concentration of NaOH of 10 M are fixed for all mixtures.

Table 3. 6. Mix design parameters

Mix ID	Curing Method	GGBFS/FA	BOFS/Sand	AAS content
M1	Steam curing 6 hours	40/60	100/0	2
M2			75/25	
M3			50/50	
M4	Steam curing 12 hours	40/60	75/25	2
M5			50/50	
M6	Ambient air curing	40/60	75/25	2
M7			50/50	
M8	Water curing	40/60	75/25	2
M9			50/50	
M10	6-hour CO_2 curing (Steam curing 6 hours)	40/60	75/25	2
M11	12-hour CO_2 curing (Steam curing 6 hours)			
M12	24-hour CO_2 curing (Steam curing 6 hours)			
M13	6-hour CO_2 curing (Steam curing 12 hours)	40//60	75/25	2
M14	12-hour CO_2 curing (Steam curing 12 hours)			
M15	24-hour CO_2 curing (Steam curing 12 hours)			

3.3. Mixing and Casting

The production of good-quality geopolymer mortar is highly dependent on the mixing process. Three mixes are prepared, with BOFS to sand ratio of 100/0, 75/25, and 50/50. Mix 2 is the same mixture as M4, M6, M8, M10, M11, M12, M13, M14, and M15, where the main difference is their curing regimes. Similarly, Mix 3 is the same as M5, M7, and M9, with four different curing regimes applied to each mixture type. The proportions of each substance are displayed in Table 3.7.

Table 3. 7. Final mix designs (kg/m³)

	M1 (100/0)	M2 (75/25)	M3 (50/50)
FA	550.7	546.4	542.2
GGBFS	367.1	364.3	361.5
BOFS	611.8	455.3	301.2
Sand	0	151.8	301.2
NaOH (10M)	122.4	121.4	120.5
Na_2SiO_3	244.7	242.8	240.9
Water	146.5	136.6	126.9

The mixing procedure starts with material preparation. Each component of the mixture is weighed and stored. First, 10 M NaOH is prepared by dissolving the NaOH pellets in water

in accordance with NaOH molar weight. Then, AAS is prepared one day before the mixing process, combining the 10 M NaOH and Na_2SiO_3.

The geopolymer mixing procedure is carried out according to the procedure specified in ASTM C305 (2015) standard specification in the Hobart mixer, as shown in Figure 3.10. First, GGBFS and FA are placed in the mixer bowl and mixed for 30 seconds at a low speed, then AAS and water are added to raw binder materials and mixed for a further 1 minute at a low speed. Next, sand and BOFS are added to the binder paste and mixed for 1 minute at a low speed. Then, hand mixing is carried out for 1.5 minutes, and for 2 minutes, the geopolymer mortar is mixed at a high speed in the mixer.

Geopolymer mortar hardens relatively quickly; thus, the casting process is carried out quickly. Before pouring each mold, the mortar paste is thoroughly mixed with the spoon to prevent the settlement of particles at the bottom of the mixer bowl.

Figure 3.10: Hobart mixer (4.7 L)

According to Table 3,8, each mixture is prepared based on the total volume specified. The total volume is calculated based on the specific mold's dimensions and the required number of samples. Additionally, 10% is added to the mix's total volume to prevent material shortage due to its loss during the casting process.

The molds filled with geopolymer mortar paste were demolded after 2 hours. Further, samples are stored at ambient air conditions for 1 day before exposure to specific curing regimes.

Table 3. 8: Quantity of samples and mixture volume estimation

Description	Tests			
	Compressive strength	Dielectric constant	Drying shrinkage	1M NaOH and water expansion
Size (mm)	50×50×50	70×70×70	25×25×285	25×25×285
Number of specimens	16	2	4	8
Testing age	3, 7, 28 and 56-day	3, 7, 31-day interval	3, 7, 31-day interval	3 and 7-day interval
Volume (m^3)	2.000×10^{-3}	0.686×10^{-3}	0.712×10^{-3}	1.425×10^{-3}
Total volume (m^3)	$(4.823\times10^{-3}) \times 10\% = 5.305\times10^{-3}$			

3.4. Curing

The effects of four different curing regimes are compared on the geopolymer mortar's mechanical, durability, and microstructural properties. Steam curing for 6 and 12 hours is carried out in the steam curing chamber shown in Figure 3.11. The steam temperature is set up at 80 ℃, and the water is filled out in the steam generator each hour. Sample mixtures 1, 2, and 3 are steam cured for 6 hours, and mixtures 4 and 5 are steam cured for 12 hours.

Ambient air-curing is carried out at room temperature (25 ± 1℃) for a day after geopolymer casting and demolding for mixture samples 6 and 7. Water curing is carried out in water storage tanks according to the ASTM C511 standard specification. Lime is added to the portable water to prevent the leaching of calcium from the geopolymer structure. Mixtures 8 and 9 are water-cured at the ambient temperature condition before test day to test the hardened properties of the geopolymer. For testing the durability properties of mixtures 8 and 9, samples were immersed in the water for a 7-day period.

Figure 3.11: Steam curing chamber and steam generator

Mixtures 10, 11, and 12 are steam-cured for 6 hours and further carbonized in the carbonization chamber for 6, 12, and 24 hours, respectively. Mixtures 13, 14, and 15 are steam-cured for 12 hours, and further carbonized in the carbonization chamber for 6, 12, and 24 hours, respectively. The carbonization chamber is shown in Figure 3.12. The temperature is set up at 23℃, humidity at 50%, and CO_2 concentration at 20%.

Figure 3.12: Carbonization chamber

3.5. Testing Procedures

3.5.1. Flowability test

The flowability of each mixture is identified during the mixing stage according to the ASTM C1437 standard specification. Figure 3.13 shows the flow table, cone, and tapper used to identify the flowability of the mixture. The mixture is poured into the cone in 2 layers and tapped 20 times. The top of the cone should be flattened, and the cone should be removed. The flow table should be dropped 25 times in 15 seconds, and the diameter of the spread

mortar is measured to identify the relative flowability value (Γ_m), presented in Equation (3.5). The high relative flowability value indicates the more flowable mortar sample.

$$\Gamma_m = \frac{\left(d_1 \times d_2 - d_0^2\right)}{d_0^2} \tag{3.5}$$

Where, d_0 is the cone diameter (bottom part), d_1 and d_2 are the diameter of the mortar.

Figure 3.13: Flow table test

3.5.2. Air content test

An air content test is conducted to understand whether the hydraulic cement mortar meets the air-entraining or non-air-entraining requirements specified before the testing. The test is conducted according to the ASTM C185 (2013) standard specification. A cylindrical unit measure of 400 ml (Figure 3.14) is filled with mortar in 3 layers and tapped 20 times per layer. The air content of the mortar is calculated by Equation (3.6). The weight of the empty cylindrical unit is measured, and the weight with poured mortar is measured to calculate the actual weight of mortar W. P is the percentage of mixing water used for mortar preparation based on the quantity of the cement. Various factors can affect air content value, such as mortar mixture proportion, compaction degree, and cementitious material's chemical content.

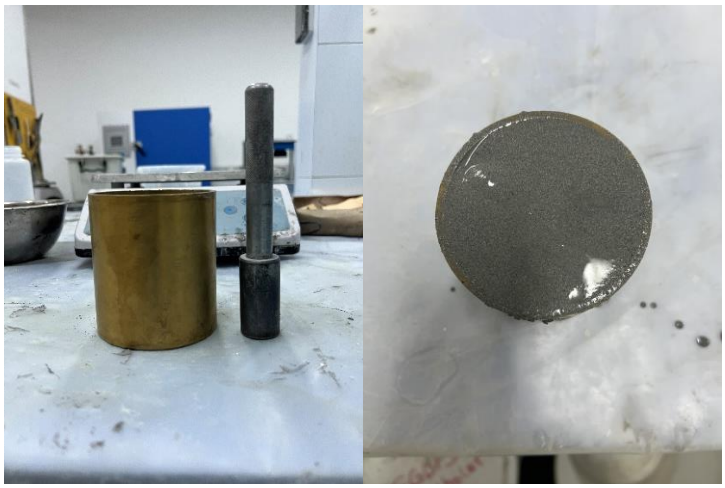

Figure 3.14: Cylindrical unit measure (400 ml)

$$Air\ content\left(vol.\%\right)=100-W\left(\frac{182.7+P}{2000+4P}\right) \tag{3.6}$$

3.5.3. Compressive strength test

For the compressive strength test, four cube samples are prepared per mixture and test day (3, 7, 28, and 56 days). The compression and bending testing machine and cube samples were used to determine the compressive strength values of each mixture, as shown in Figure 3.15. The test is conducted according to the ASTM C109 standard specification.

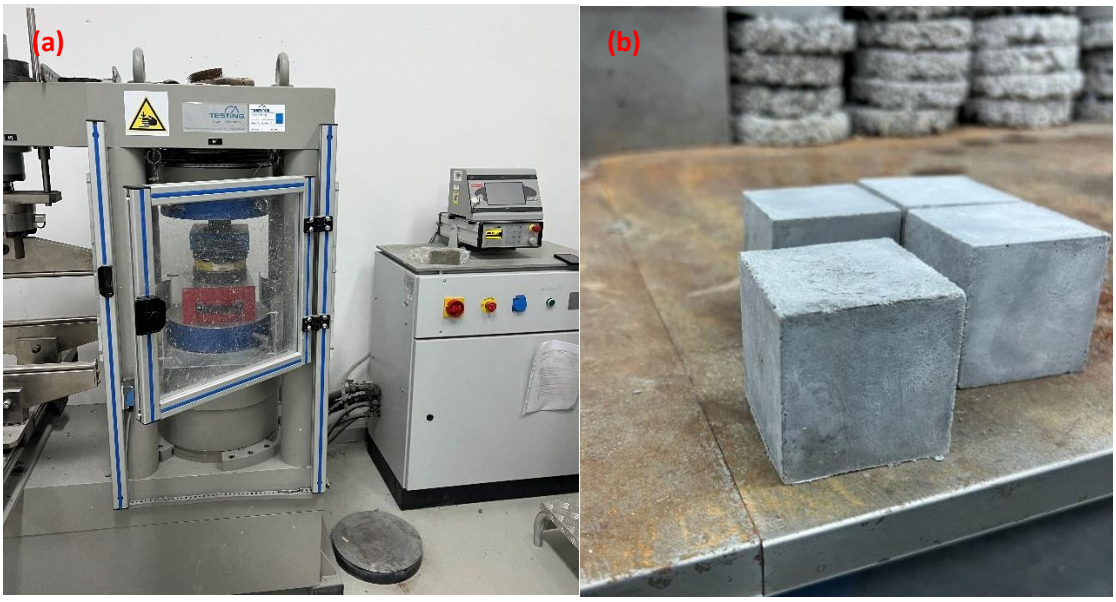

Figure 3.15: (a)Compression and bending testing machine of concrete samples; (b)samples with 50x50x50 mm dimensions

3.5.3. Dielectric constant test

The dielectric constant test was carried out on two samples with 70x70x70 mm dimensions per each geopolymer mixture type. Figure 3.15(a) illustrates the apparatus and Perconnect software used to measure the dielectric constant of geopolymer mortar samples. The test was conducted for 6 months, increasing periodicity from 3 to 7 days. The sides of the cube were numbered, and the dielectric constant of each side was measured. Thus, for the analysis, the mean value was employed.

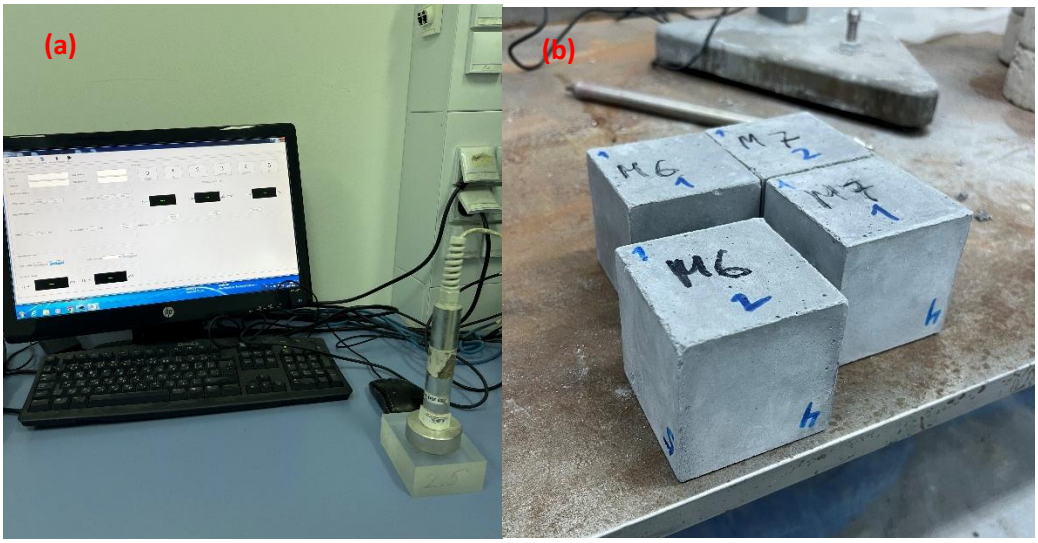

Figure 3.16: (a) Dielectric constant test equipment and software; (b) samples with 70x70x70 mm dimensions

3.5.5. Drying shrinkage test

The ASTM C596 (2010) standard specification was followed in conducting the drying shrinkage test to identify the length and mass loss of mortar bar pieces during the 6 months of testing. Four bar samples are prepared per mixture and air-dried at a specific temperature and relative humidity of 20 °C and 65%, respectively. Figure 3.17 shows the comparator with a digital display used to measure the length change and scale to measure the weight change of bar samples. The purpose of conducting a drying shrinkage test on the mortar samples is to understand the possible behavior of the concrete samples prepared with the same materials and cured under the same conditions.

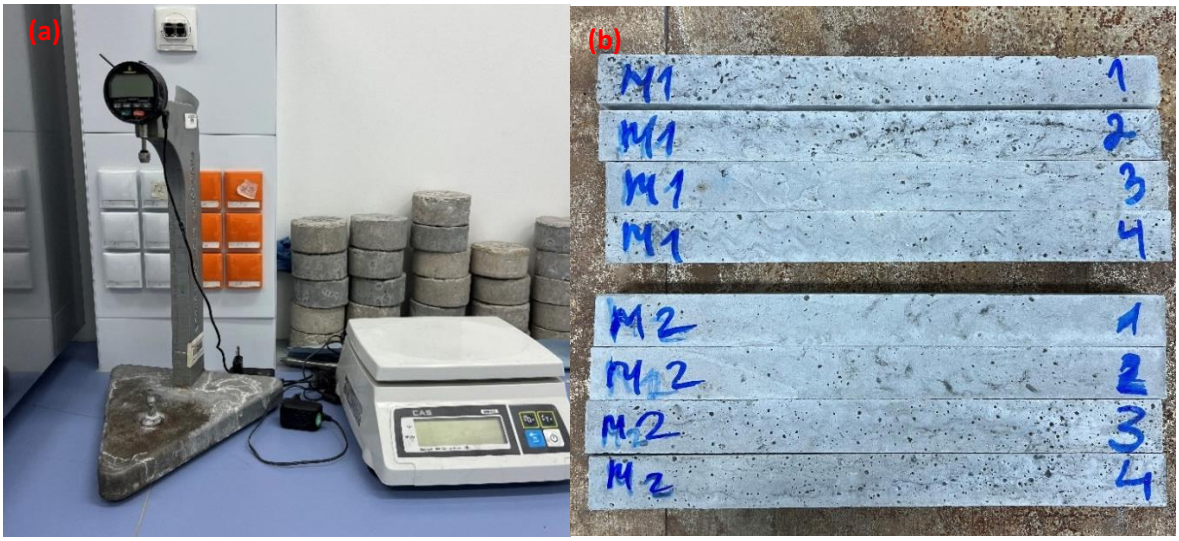

Figure 3.17: (a)Comparator with digital display for measuring drying shrinkage (ASTM C596) and scales; (b)samples with 285x25x25 mm dimensions

3.5.6. 1 M NaOH and Water expansion test

The alkali-silica reaction resistance of the mortar samples was tested by immersing the bar samples in 1M NaOH solution, whereas the water expansion as a result of the creation of $Ca(OH)_2$ was tested by immersing the bar samples in water. The ASTM C1260 standard specification was followed in conducting the test. After the specified curing period, the pre-reading of the bar length was measured using a comparator with a digital display (Figure 3.18 (a)). The bar samples were immersed in the water and spent a full day in the oven at 80 °C temperature. The bar specimens were then submerged in a 1M NaOH solution, and the length change was noted until the conclusion of the 28 days. The water expansion test was continuously carried out in water storage tanks placed in the oven at 80 °C temperature. The purpose of the ASR resistance and water expansion tests is to detect the aggregate of its potential expansion behavior while submerging in NaOH solution or water.

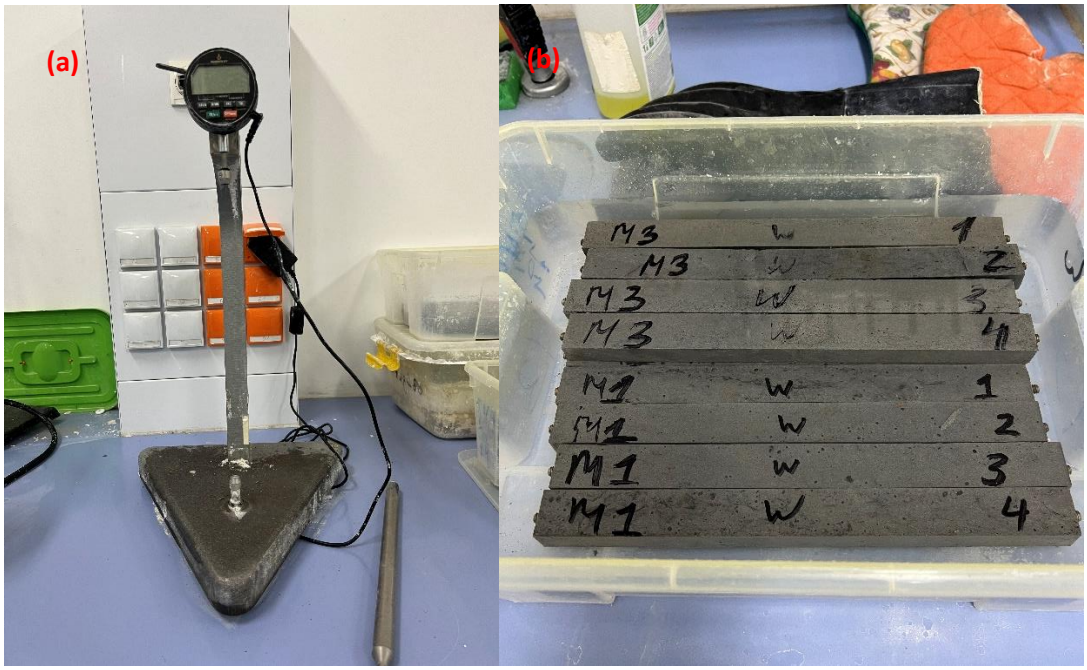

Figure 3.18: (a)comparator with digital display for measuring expansion (ASTM C1260); (b)samples with 285x25x25 mm dimensions

3.5.7. X-ray diffraction (XRD)

The chemical composition of geopolymer mortar samples was tested using the X-ray diffraction (XRD) system (SmartLab Rigaky apparatus), as illustrated in Figure 3.19 (a). Prior to the testing procedure, the geopolymer mortar samples are crushed and shredded into the powder. The powder from the #200 sieve size was used to analyze the geopolymer's chemical composition. The range of X-ray scanning was conducted from 10 to 70^{o} (2θ) at a specified increment of 0.01^{o}. Figure 3.19 (b) illustrates the geopolymer powder capsules that were placed in the XRD apparatus. The XRD results were further analyzed using MDI Jade 6 software to identify the peaks.

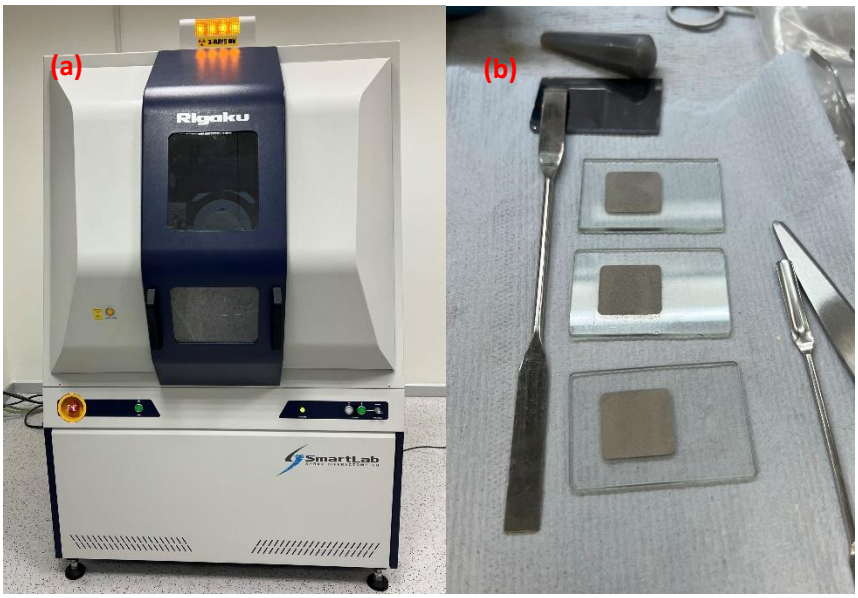

Figure 3.19: (a)X-ray diffraction equipment; (b)geopolymer powder samples

3.5.8. Scanning electron microscope (SEM) image

The scanning electron microscope (SEM) image of crushed geopolymer samples was investigated using the ZEISS Crossbeam 540 apparatus (Astana, Kazakhstan), shown in Figure 3.20. Since the geopolymer mortar samples have poor electrical conductivity, crushed samples were coated with gold with a thickness of 10 nm. The coating procedure was carried out using the Sputter-coater Q150T ES apparatus. An SEM image was used to investigate the inner structure of the geopolymer and determine its composition and physical characteristics, which were magnified under a microscope.

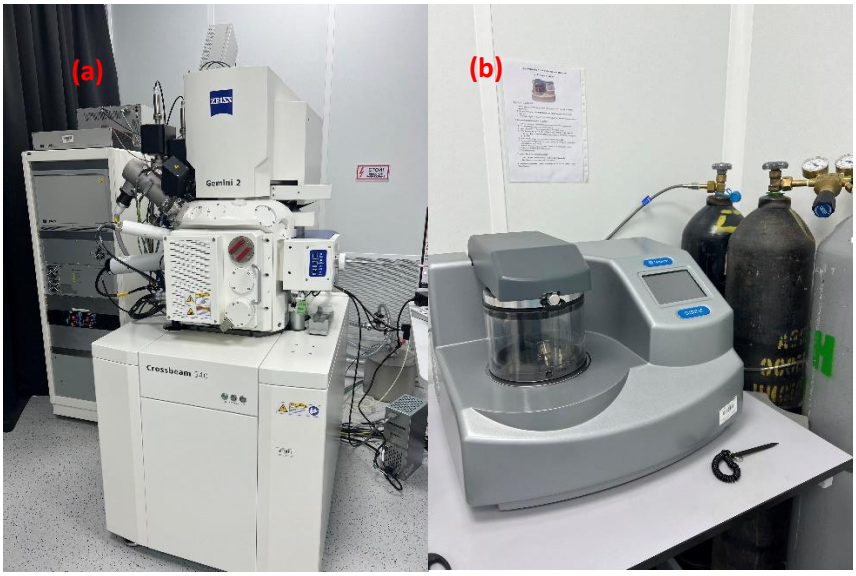

Figure 3.20: (a)SEM apparatus; (b)coating equipment

3.5.9. Fourier transform infrared spectroscopy (FTIR) analysis

Figure 3.21 shows the Nicolet iS10 FT-IR Spectrometer (Kazakhstan, Astana) apparatus used to conduct FTIR analysis on geopolymer samples. The geopolymer mortar samples were crushed and powdered. The powder sample passing through the #200 sieve size (75 μm) was utilized for the following analysis. The absorbance spectra and transmittance mode were set in the range of 400 to 1400 cm^{-1}. The recorded data is displayed in OMNIC software.

Figure 3.21: (a)Nicolet FTIR Spectrometer

Chapter 4 - Results and Discussion

4.1. Fresh Properties

4.1.1. Flowability test

Figure 4.1 presents the geopolymer mortar mixture's relative flowability (Γ_m) test results for replacing basic oxygen furnace slag (BOFS) with river sand. The Γ_m value of geopolymer mortar mixtures varies in the range of 3.6 to 4.4. Generally speaking, when the amount of BOFS aggregate in the mixture increases, the Γ_m decreases because BOFS aggregate has a higher angularity than river sand. The geopolymer mortar mixture containing 100% BOFS aggregate shows the smallest Γ_m despite the higher specific gravity of BOFS aggregate. It is well known that the aggregate with a high specific gravity increases the total binder content of the mortar mixture. Thus, the higher binder content in the mortar mixture covers and surrounds the aggregate surface, increasing the flowability of the mortar mixture [93]. However, the mortar mixture containing 100% BOFS aggregate with higher specific gravity than sand presents the opposite trend. The porous nature of the BOFS may cause this result. In the geopolymer mortar mixture with 100% BOFS aggregate, binder paste is partially absorbed onto the aggregate surface rather than covering it. Thus, Γ_m is relatively low.

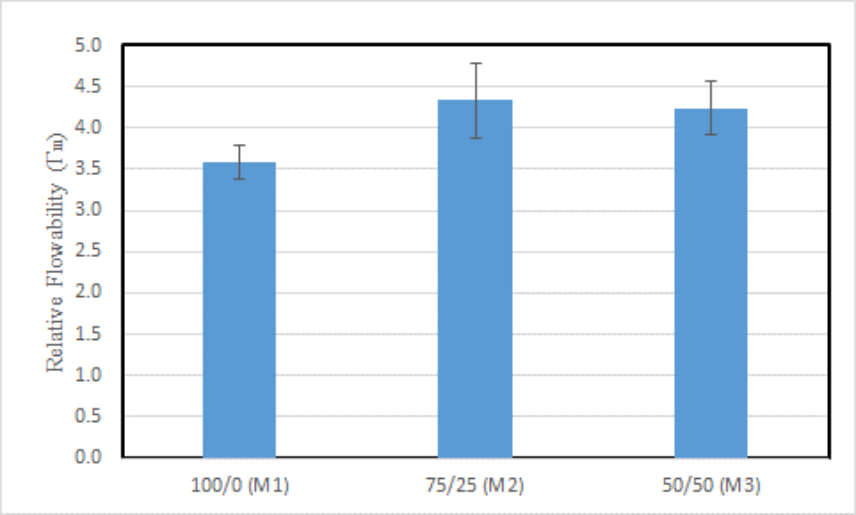

Figure 4.1: Relative flowability test results of geopolymer mortar mixtures

Interestingly, the geopolymer mixture with the combined 50% BOFS and 50% sand shows a slightly lower Γ_m value than the combined 75% BOFS and 25% sand. This result may be attributed to the combined effect of aggregate angularity and binder content due to the aggregate's specific gravity. When BOFS and sand are used together, the binder content effect seems more dominant than the aggregate angularity effect because small sand particles may fill BOFS voids.

4.1.2. Air content test

The geopolymer mortar mixture's air content is shown in Figure 4.2. The air content value in geopolymer mortar mixture varies from 18 to 20.5%. The air content of mixtures increases with the decrease of BOFS aggregate content. Such a pattern might be observed due to the pozzolanic reaction between f-CaO and AAS in the geopolymer matrix. The reaction products formed during the polymerization reaction fill the voids and harden, thus decreasing the air content. Geopolymer mortar mixture containing 100%BOFS aggregate has a higher content of f-CaO. Thus, the formation of C-S-H and C-A-S-H gel is higher, which leads to lower air content value due to explicit void fills. The decrease in BOFS amount increases the air content of the geopolymer mortar mixture, as the voids are filled less due to the lesser amount of geopolymer gel formed.

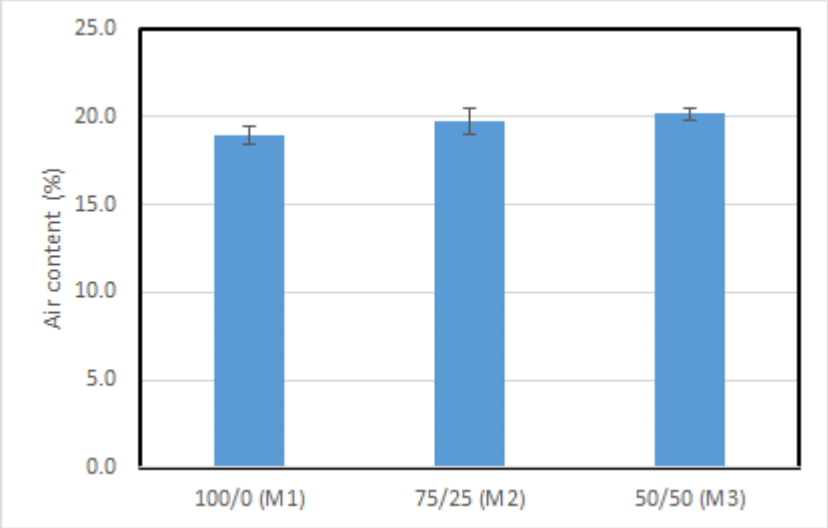

Figure 4.2: Air content of geopolymer mortar mixtures

4.2. Hardened Properties

4.2.1. Compressive strength

The compressive strength development of 6- and 12-hour steam-cured geopolymer samples is shown in Figures 4.3 (a) and (b). The compressive strength values vary in the range of 30 to 40 MPa, which is substantially higher than the compressive strength of air- and water-cured samples (Figure 4.4). Overall, the longer duration of steam curing positively affected only the initial compressive strength of mortar samples. Thus, the compressive strength value is 31 MPa and 35 MPa at 3 days and 34 MPa and 36 MPa at 7 days for 6- and 12-hour steam-cured geopolymer mixtures, respectively. The 28-day and 56-day compressive strength values for 6 h and 12 h steam curing are similar. According to Zeyad [72] and Yunsheng [100], the higher temperature and longer duration of steam curing increase the polymerization rate in the geopolymer mixture, thus increasing the compressive strength of the mixtures. The results show an increase in compressive strength from 3 to 28 days. Further, from 28 days to 56 days of age, a reduction in compressive strength is observed, which correlates with the findings of other studies [93]. Large amounts of silicon and aluminum in the geopolymer raw material support the increase in compressive strength up to 28 days of age. However, the reduction of the components mentioned above in the geopolymer structure ceases the further increase of compressive strength.

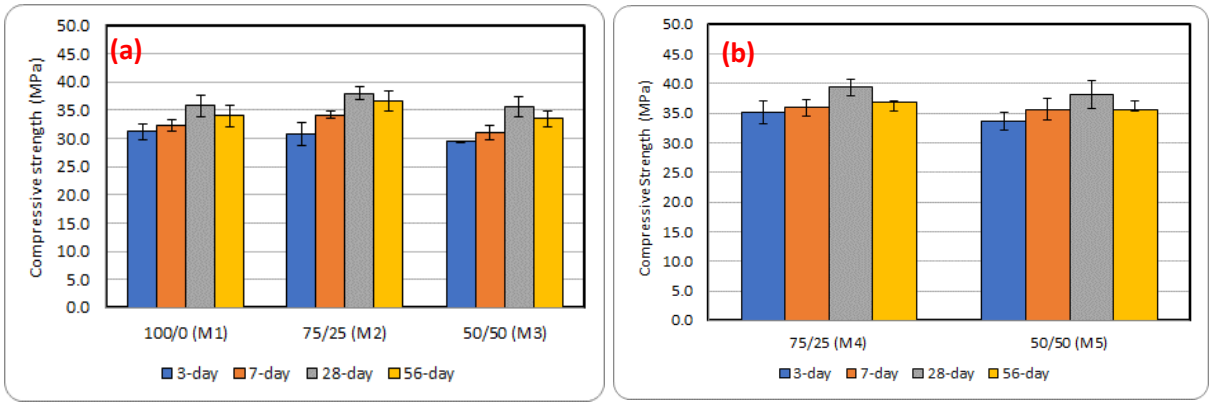

Figure 4.3: Compressive strength (a) Steam curing 6 hours; (b) Steam curing 12 hours

It is noteworthy that the 100% BOFS mixture (M1) develops the highest initial (3-day) compressive strength, but further development is lower in comparison to the mixture containing 25% Sand (M2), which might be attributed to the expansive characteristic of BOFS aggregate. The higher substitution of BOFS with Sand (50%) resulted in lower initial and final compressive strength values. Such a pattern is related to the poor bond connection

between paste and aggregate in geopolymer matrix systems containing sand. It should be noted that BOFS has an angular and rough texture, while sand is angular and smooth.

The compressive strength development for ambient air-cured and water-cured samples is displayed in Figures 4.4 (a) and (b), respectively. Ambient air-cured mixtures exhibit high-early strength development of 18 to 22 MPa compared to water-cured mixtures (15 MPa). The lower strength in water-cured mixtures at an early age may be due to decreased AAS concentration. When geopolymer mortar samples are submersed into water (water-curing), sodium ions (Na^+) in the geopolymer mixture leach out (dissolution of Na), thereby leading to disruption of polymerization and less strength gain eventually [71]. However, further compressive strength development is apparent in water-cured mixtures, while the strength of ambient air-cured samples decreases. It may be attributed to the micro-cracks in the mixture matrix associated with forming $Ca(OH)_2$ and Mg $(OH)_2$ from BOFS aggregate. Compressive strength drops at the 56-day testing period except for water-cured geopolymer mixtures. Overall, the continuous increase of compressive strength is noticeable for water-cured mixtures. Since the continuous hydration process occurs in the water-cured geopolymer mortar samples, the compressive strength value keeps increasing until 56 days of testing. Termkhajornkit [86] reported that continuous water curing contributes to a higher degree of continuous hydration of the mixture containing FA and GGBFS. It is well known that strength development stops when moisture required for cement hydration is no longer available. The air-cured samples lose moisture due to water evaporation, and less water is available for further hydration to increase the strength. In the case of ambient air-cured mixtures, the pattern of compressive strength development is similar to steam-cured mixtures.

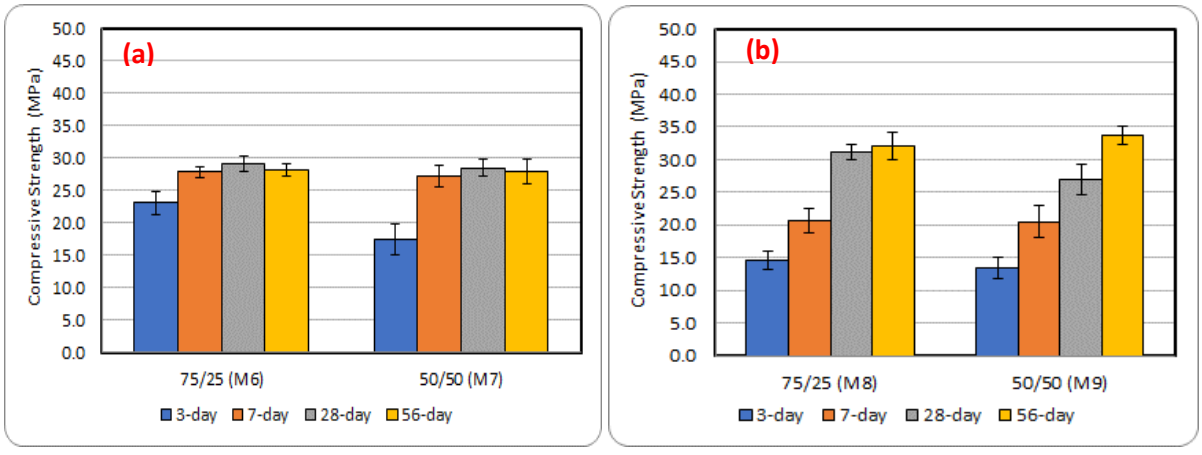

Figure 4.4: Compressive strength (a) Ambient air curing; (b) Water curing

In the case of ambient air-cured mixtures, the mixture containing 75%BOFS develops high-early strength compared to the mixture containing 50%BOFS. This result correlates with steam-cured mixtures and is related to the bond connection. Water-cured mixtures show relatively similar compressive strength results regardless of the BOFS/Sand ratio difference.

Figures 4.5 (a) and (b) show the compressive strength development of CO_2-cured mixtures in combination with steam curing for 6 and 12 hours, respectively. The combined steam- and CO_2-curing has a slightly lower initial early-age compressive strength (at 3 days) but favors the 28- and 56-day compressive strength value compared to simply steam-cured mixtures. The continuous increase of compressive strength until 28 days and further decrease is visible from the illustration. Mixtures M10 and M13 are CO_2 cured for 6 hours and obtained compressive strength of 38 and 40 MPa at the testing period of 28 days, respectively. Mixtures M11 and M14 were CO_2 cured for 12 hours and obtained compressive strength of 39 and 43 MPa at the testing period of 28 days, respectively. Mixtures M12 and M15 were CO_2 cured for 24 hours and obtained compressive strength of 40 and 45 MPa at 28 days, respectively. Overall, a longer duration of CO_2 curing produces higher compressive strength than a shorter duration of CO_2 curing. These results may be explained by the formation of calcium carbonate from calcium silicate's reaction with CO_2 after a certain period [90].

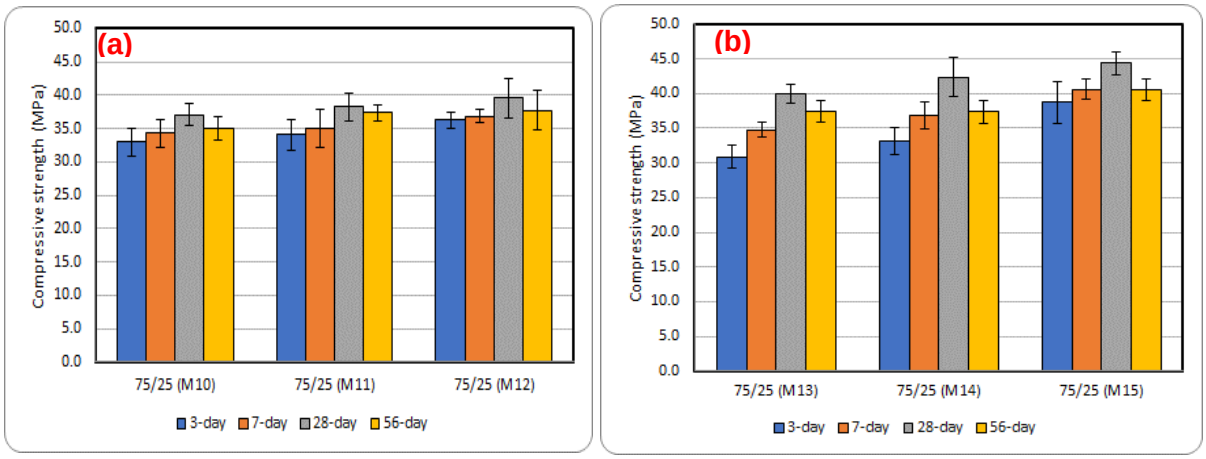

Figure 4.5: Compressive strength (a) 6hr Steam + 6,12,24hr CO_2 curing; (b) 12hr Steam + 6,12,24hr CO_2 curing

4.2.2. Dielectric constant

The dielectric constant test results are shown in Figures 4.6 to 4.8. Overall, it can be observed that the dielectric constant tends to decrease with increasing time. This pattern is related to moisture loss from the geopolymer mortar matrix system. Thus, the continuous water-cured mixture results in Figure 4.7(b) show the steady dielectric constant value over the

testing period, as no moisture loss occurs. The dielectric constant value is related to the geopolymer concrete's compressive strength and hydration reaction process.

Figures 4.6 (a) and (b) show the change of dielectric constant value with age for 6- and 12-hour steam-cured mixtures, respectively. A sharp decrease in dielectric constant value was observed during the first 28-day period. Further, a smooth decline was observed. This pattern correlates with the compressive strength result, showing that the hydration and geopolymerization processes are carried out during the first 28 days. The dielectric constant value of both 6- and 12-hour cured samples is relatively the same. The high temperature of steam curing induces more rapid electrically resistive gel formation in the geopolymer matrix. In steam-cured samples, fewer unreacted particles are left, and the geopolymer structure is denser; consequently, a smaller decrease in the dielectric constant is observed. The steam-cured mixtures have higher dielectric constant values of 15-13 at the age of 186 days compared to air-cured mixtures of 10-11 at ambient temperature.

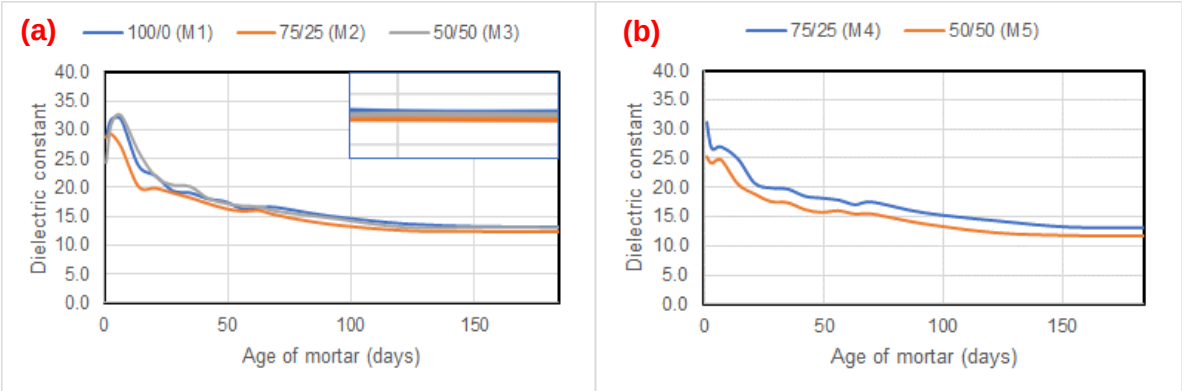

Figure 4.6: Dielectric constant (a) Steam curing 6 hours; (b) Steam curing 12 hours

The dielectric constant value change for ambient air- and water-cured mixtures can be observed in Figures 4.7 (a) and (b), respectively. The dielectric constant value for the water-cured mixture decreases during the first week of curing. However, further, the dielectric constant value increases and is stabilized. The initial decrease of dielectric constant value is attributed to Na^+ ions leaching from AAS and its dissolution in water. However, the dielectric constant value is further stabilized due to the continuous hydration process in the water-cured mixture, which is continuously immersed in water. In the case of ambient air-cured mixtures, the sudden increase of dielectric constant value occurs at the 7-day curing, which might be attributed to the pore water consumption by unreacted particles. Further, a sharp decrease is observed in the 7-28 day period, which indicates the hydration reaction occurring in the geopolymer matrix.

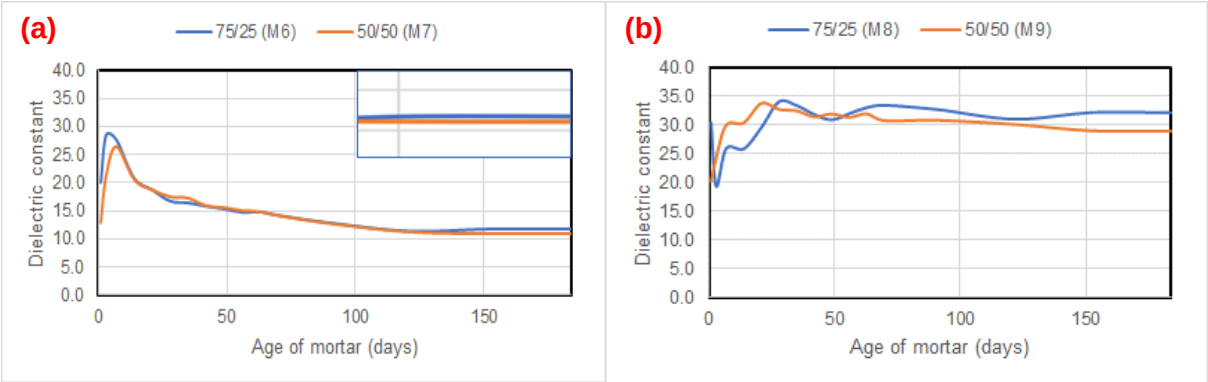

Figure 4.7: Dielectric constant (a) Ambient air-curing; (b) Water curing

Figures 4.8 (a) and (b) show the change of dielectric constant value for 184-day period for CO_2 cured samples in combination with steam for 6 and 12 hours, respectively. The CO_2 curing in combination with steam curing resulted in the decrease of dielectric constant value. According to Chuewangkam [101], carbon affects the electrical conductivity of the geopolymer matrix by reducing the dielectric constant. From Figure 4.8, it might be observed that the dielectric constant value varies from 10 to 11. However, it should be noted that the duration of CO_2 curing does not affect the 12-hour steam-cured specimen, while the 6-hour steam-cured specimens are affected by different CO_2 curing duration. The highest dielectric constant of 14 is obtained for the 6-hour CO_2 curing duration, which correlates with Chuewangnkam's findings [101] that the carbon reduces the dielectric conductivity of geopolymer mortar. The geopolymerization reaction in the 12-hour steam-cured mixture is accelerated and almost completed by the time when CO_2 curing is applied. Thus, there is less effect on the dielectric constant from CO_2 incorporation.

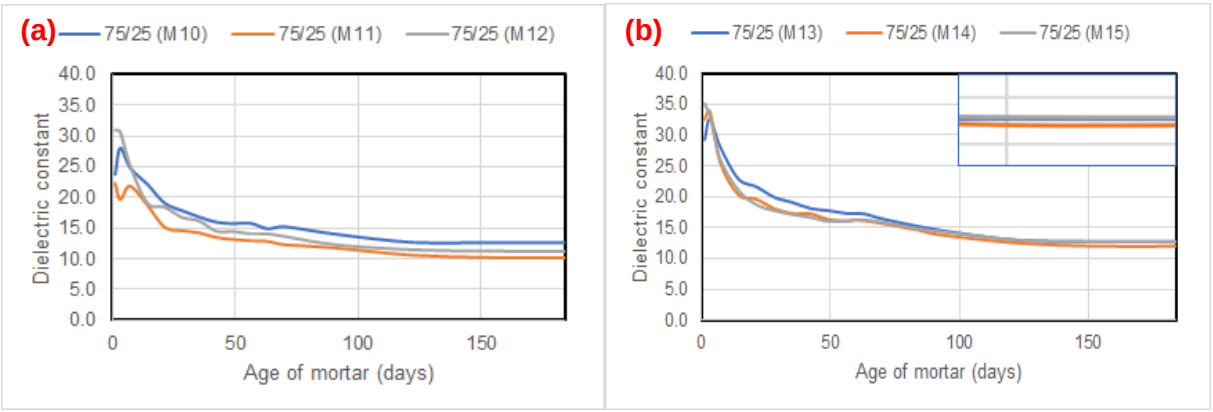

Figure 4.8: Dielectric constant (a) 6hr Steam + 6,12,24hr CO_2 curing; (b) 12hr Steam + 6,12,24hr CO_2 curing

4.3. Durability

4.3.1. Shrinkage strain

Figures 4.9 and 4.10 show the drying shrinkage (length change) and mass loss for the mixtures of steam-cured for 6 and 12 hours, respectively. Test results present that the longer duration of steam curing leads to less length shrinkage and mass loss, which is related to the faster polymerization rate in the geopolymer mixture, eventually forming denser structures in the geopolymer mixture. Thus, mortar mixtures containing 75% BOFS show 0.3% and 0.13% drying shrinkage and 9.5% and 5.2% mass loss for 6- and 12-hour steam-cured conditions, respectively. Overall, the mixtures containing 75% BOFS show a lower shrinkage rate than mixtures containing 50% BOFS and 100% BOFS. For example, the 6-hour steam-cured specimens have drying shrinkage values of 0.32% (100% BOFS), 0.25% (75% BOFS), and 0.29% (50% BOFS) for the 184-day testing period. The mixture with 100% BOFS has higher drying shrinkage because of the porous structure of BOFS. The excess water is absorbed by BOFS particles, thus mainly causing the negative pressure in capillaries. The mixture with 50% BOFS has poor bond connection due to the round and smooth texture of the sand, which also influences higher drying shrinkage. The primary cause of shrinkage is the creation of negative pressure in the capillary framework of the geopolymer [76]. The drying shrinkage rate for steam-cured mixtures is relatively low compared to air-cured ones. The condensation process in geopolymer samples, which is associated with the moisture loss from capillaries, is accelerated by steam curing. Thus, significant drying shrinkage occurs at the initial stage of curing, and further on, it is stabilized.

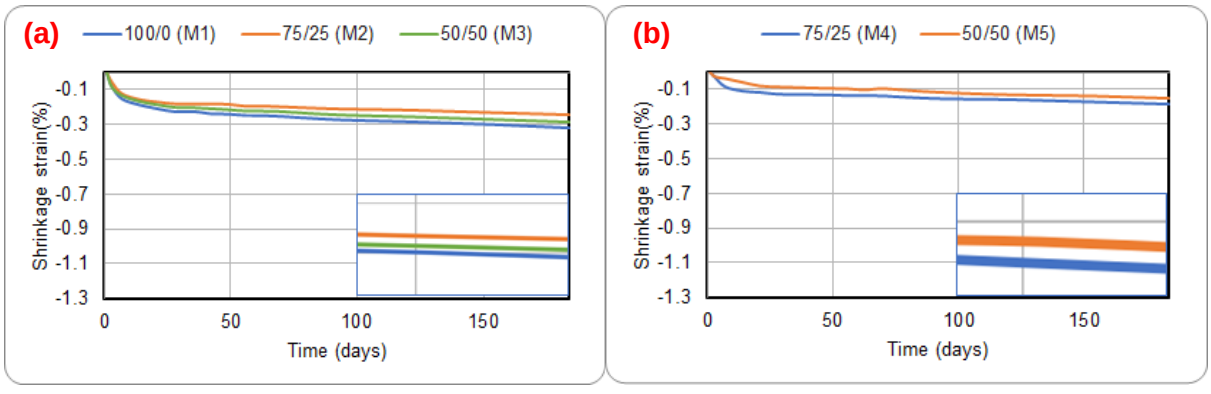

Figure 4. 9: Drying shrinkage length change (%): (a) Steam curing 6 hours; (b) Steam curing 12 hours

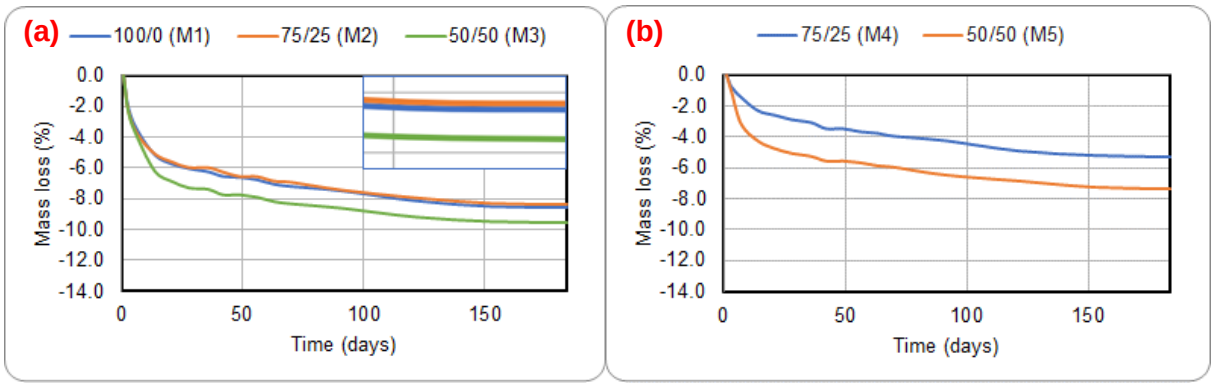

Figure 4. 10: Drying shrinkage mass loss (%): (a) Steam curing 6 hours; (b) Steam curing 12 hours

Water- and air-cured mixtures at ambient temperature exhibit the highest shrinkage strain compared to mixtures cured under other curing conditions. Such a pattern is observed due to excess pore water evaporation. Under steam-cured conditions, the condensation process is accelerated. As a result, excessive drying shrinkage occurs at the initial stage of the drying process and is then stabilized [76]. According to Figure 4.11, the water-cured mixtures (1.1-1.2%) undergo more significant drying shrinkage in comparison to air-cured mixtures (1-1.05%), which might be due to the excess water infiltration in the micropores of mixture specimen during the water curing process. The mass loss for both water- and air-cured mixtures is shown in Figure 4.12. The water-cured mixtures exhibit a higher drying shrinkage of 13% compared to air-cured samples of 8%. During the water curing, the water-cured mixtures absorb and store the water on the surface and in the inner structure of the geopolymer. The water amount and drying shrinkage have a linear relationship. Thus, increasing the water content will simultaneously increase the drying shrinkage of the geopolymer mixture. Similarly to steam-cured mixtures, the BOFS to sand ratio of 75/25 shows comparatively less drying shrinkage compared to the ratio of 50/50, proving the statement of better bond interlocking in BOFS particles, eventually influencing drying shrinkage results.

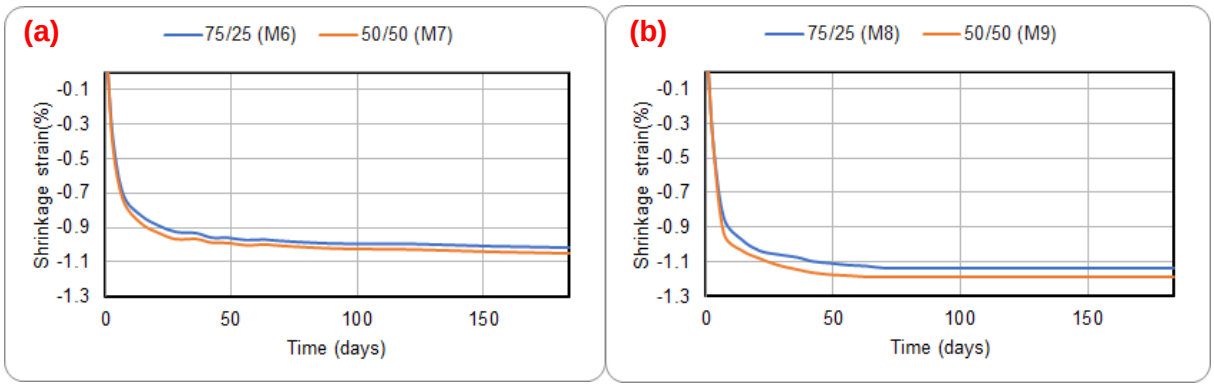

Figure 4. 11: Drying shrinkage length change (%): (a) Air curing; (b) Water curing

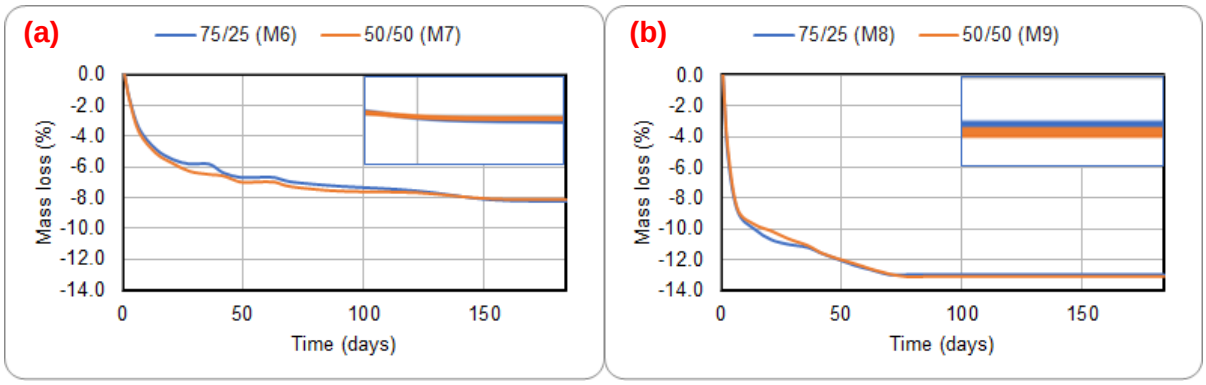

Figure 4. 12: Drying shrinkage mass loss (%): (a) Air curing; (b) Water curing

According to Figures 4.13 and 4.14, combining steam and CO_2 curings reduced the shrinkage strain of 6-hour and 12-hour steam-cured samples. However, a longer steam-curing duration combined with 24-hour CO_2 curing does not significantly change shrinkage strain. According to Figures 4.13 and 4.14, the duration of CO_2 curing has a different effect on 6-hour and 12-hour steam-cured mixtures. For example, the drying shrinkage of bare steam-cured mixtures is 0.25% at the testing period of 184 days, while the drying shrinkage values of steam-cured and CO_2 cured mixtures at the same testing period are 0.20% (6hr CO_2), 0.16% (12hr CO_2) and 0.17% (24hr CO_2). The obtained result indicates that the 12-hour and 24-hour CO_2 curing result in lesser drying shrinkage, which is correlated to the formation of stable calcium carbonate in the geopolymer matrix. In contrast, the combination of 12-hour steam and CO_2 curing gave the following results: 0.19% (bare steam), 0.17% (6hr CO_2), 0.16% (12hr CO_2), and 0.20% (24hr CO_2). Thus, 24-hour CO_2 curing is more favorable for 6-hour steam curing, and 12-hour CO_2 curing is more favorable for 12-hour steam-cured mixture.

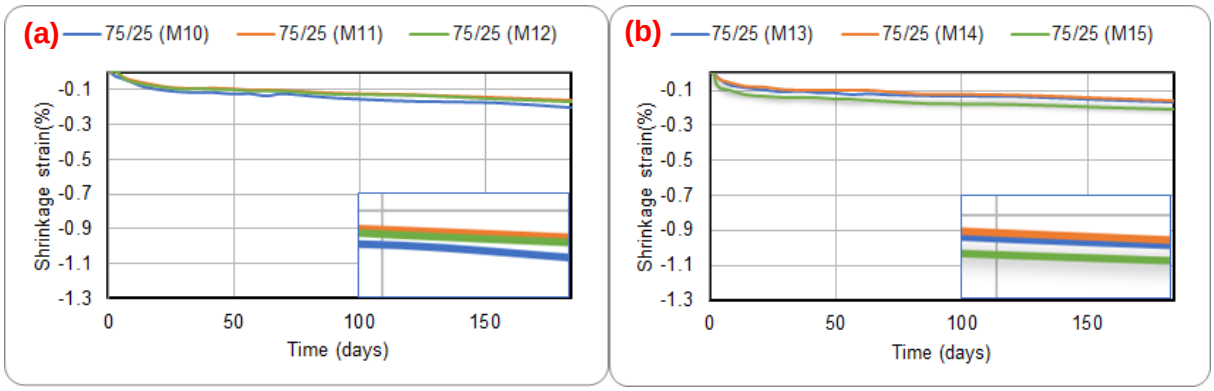

Figure 4. 13: Drying shrinkage length change (%): (a) 6hr Steam + 6, 12, 24hr CO_2 curing; (b) 12hr Steam + 6, 12, 24hr CO_2 curing

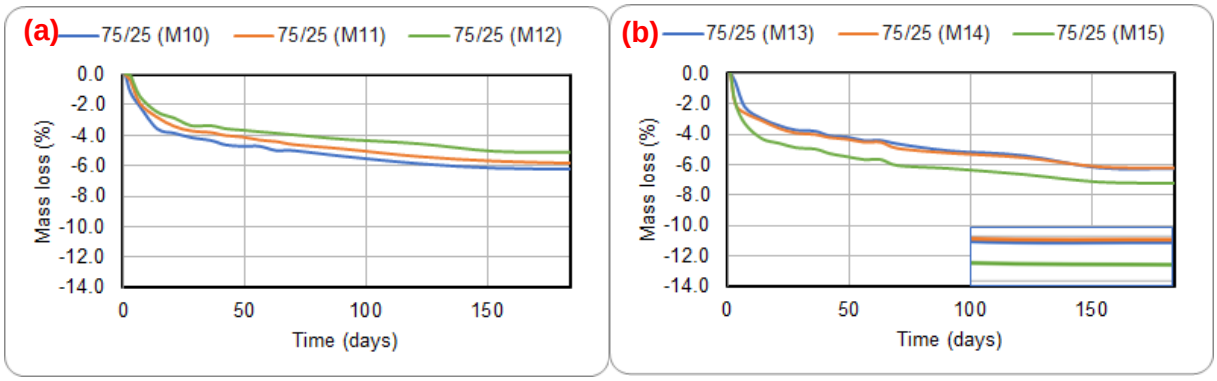

Figure 4. 14: Drying shrinkage mass loss (%): (a) 6hr Steam + 6,12,24hr CO_2 curing; (b) 12hr Steam + 6,12,24hr CO_2 curing

4.3.2. 1M NaOH expansion and water expansion

To determine whether the aggregate used in the geopolymer mixture has the expansion prospective due to $Ca(OH)_2$ and/or $Mg(OH)_2$ formation that causes the cracks in the geopolymer matrix, the expansion limit value according to ASTM C1260 is specified. In fact the C 1260 method uses 1M NaOH solution where the mortar bar sample is submersed in this solution. Thus, the mortar bar samples exceeding the expansion limit of 0.1% on the 14^{th} day of testing are considered potentially reactive at 1M NaOH solution and 80^{o}C. The expansion test conducted in this study has a few modifications. It includes two test solution conditions, 1M NaOH and water. The length change of the geopolymer mortar samples was measured up to 28 days.

The mortar bar expansion under an alkaline environment (potential alkali-silica reaction (ASR) reaction) occurring in its structure is shown in Figure 4.15. The expansion of water-cured (M8) and air-cured (M6) mixtures is relatively higher than other mixtures. The

expansion of the air-cured mixture is primarily noticed at an early age, while the expansion development of the water-cured mixture is more obvious at a later age. Mixtures M8 and M6 are potentially unreactive until 14 days, but further expansion is observed. Such a trend occurs due to the expansion nature of BOFS aggregate, where f-CaO and f-MgO form unstable compounds $Ca(OH)_2$ and $Mg(OH)_2$. CO_2 curing prevents the expansion of mortar bar samples due to the formation of stable calcium carbonate, while steam-curing prevents the expansion due to accelerating the hydration and geopolymerization process under high temperatures.

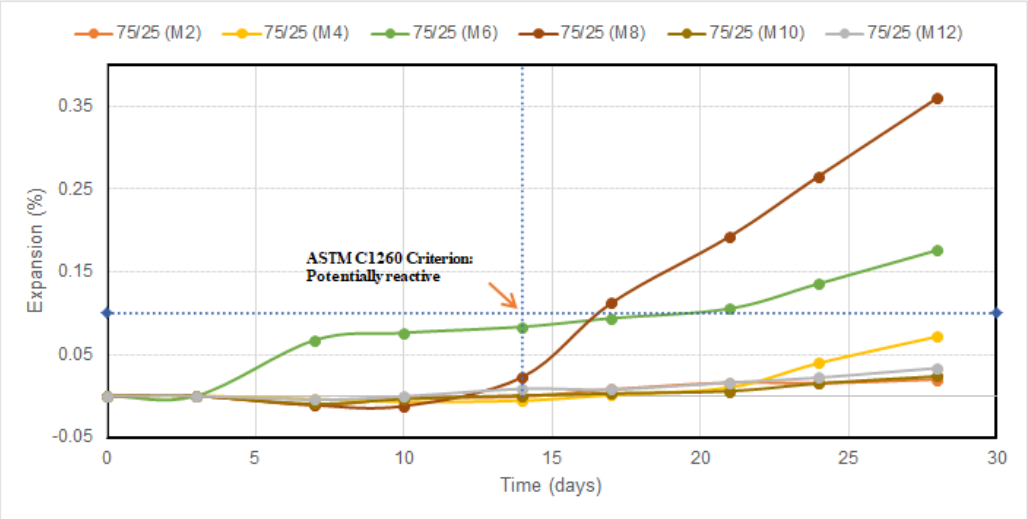

Figure 4. 15: 1M NaOH expansion

Figure 4.16 shows the water expansion results of geopolymer mortar mixtures. All mixtures do not exceed the threshold value of 0.1% (even showing shrinkage). Thus, the BOFS aggregate in the geopolymer matrix is unreactive only in a moisture environment. This correlates with the earlier statement that indicates the formation of stable compounds such as wollastonite and enstatite during the reaction between f-CaO and f-MgO with free silicon.

The effect of the curing regime on the expansion of geopolymer mixtures is negligible, but less fluctuation in length change is observed for longer curing duration for both steam and CO_2 curing.

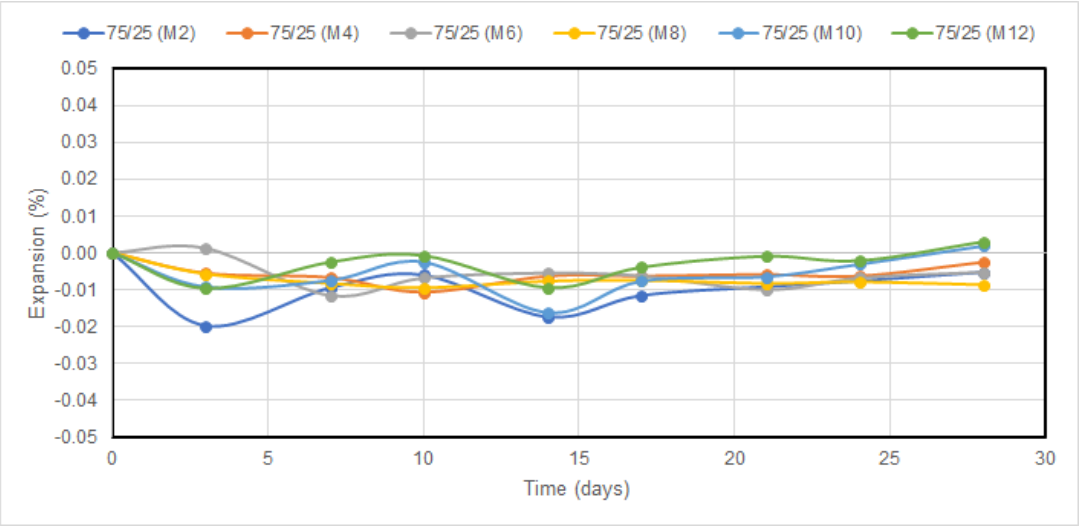

Figure 4. 16: Water expansion

4.4. Microstructural Properties

4.4.1. X-ray diffractometer (XRD) investigation

Figure 4.17 illustrates the XRD pattern of geopolymer mortar samples. The formation of quartz, mullite, larnite, calcium silicate hydrate, portlandite, gypsum, and calcite is established during XRD analysis. The formation of calcium silicate hydrate is attributed to the stabilization of BOFS-based geopolymer due to the reaction between f-CaO and free silicon. Silicon oxide peaks (quartz) reduction is observed for all curing regimes compared to forerunner material. It is a clear indicator of the reaction mechanism between AAS and silicon.

The peaks with the highest intensity are observed in the range of 25 to 30˚ of 2θ, corresponding to quartz and mullite. Steam-curing at elevated temperatures reduced quartz and mullite peak intensity (Figure 4.17), which claims that the steam curing favors the continuous chemical reaction in the geopolymer matrix.

Water-cured and air-cured geopolymer mixtures showed relatively similar results to steam-cured samples. However, the peak intensity is two times higher, as shown in Appendix Fig.1. Thus, the geopolymerization reaction is more apparent during steam-curing. Curing at elevated temperatures contributes to the formation of C-S-H gel and the dissolution of amorphous crystalline particles. The combination of steam-curing with CO_2 curing resulted in calcite formation, shown in Fig.2 (Appendix), due to the reaction between f-CaO and CO_2. Overall, the reduction of the peak intensity of quartz and mullite under steam curing and CO_2 is negligible compared to the bare steam-curing process. The obtained XRD results support

the expansion test. During the hardening process, the unreacted amorphous components of the geopolymer matrix cause internal cracks, which leads to expansion problems. The XRD analysis revealed the highest quartz and mullite peak intensities in water and ambient air-cured samples.

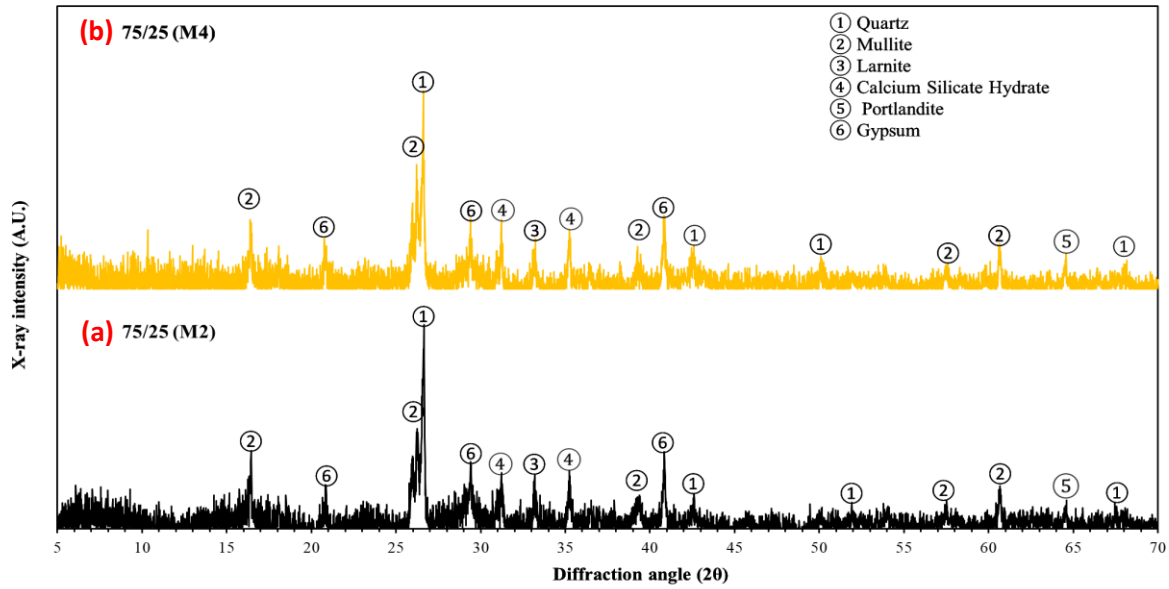

Figure 4. 17: XRD pattern of (a) Steam cured 6hr and (b) Steam cured 12hr samples

4.4.2. Scanning Electron Microscope (SEM) image analysis

The products of the alkali-activated solution reaction with the binder and aggregate are C-S-H (calcium silicate hydrate) and C-A-S-H (calcium alumina silicate hydrate) gel. The advantages of formation C-S-H and C-A-S-H are obtaining a more homogeneous and less porous geopolymer structure. Usually, C-S-H and C-A-S-H are characterized by high alumina content and low proportion of silica to calcium, which is supported by EDS analysis shown in Table 4.1. The high compressive strength of the geopolymer mixture corresponds to the strong bonding developed between aggregate particles due to C-S-H and C-A-S-H gel and the formation of a solid interfacial transition zone (ITZ).

Under the high curing temperature, geopolymer gel formation is accelerated, and the number of unreacted particles remains less, refer to Figures 4.18 - 4.20. SEM image of a 6-hour steam-cured mixture under 80℃ demonstrates the homogeneously packed and dense geopolymer structure. Under air- and water-curing conditions, unreacted fine aggregate particles and less homogeneously packed geopolymer structures can be observed. These findings correlate with Mashifana's finding [97], which states that high-temperature curing

induces a dense and uniformly packed geopolymer structure. However, curing at a high temperature induced microcrack formation in geopolymer mortar matrix because of fast geopolymerization and quick hardening, reducing compressive strength at 56 days.

Overall, the SEM image analysis revealed that the steam-curing duration does not significantly affect the microstructural properties of the geopolymer, as well as a combination of steam curing with CO_2 curing.

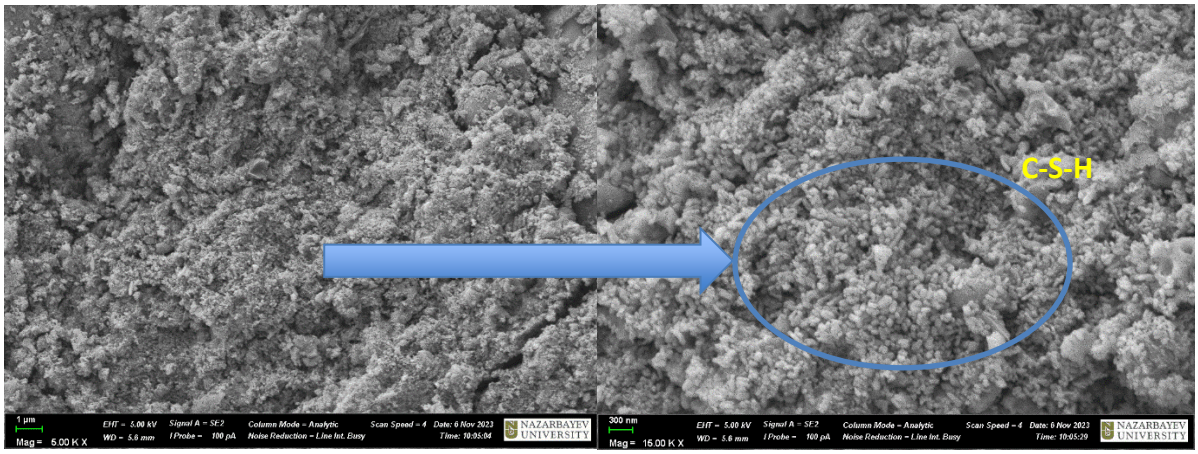

Figure 4. 18: SEM image of 6h steam cured sample 75/25 (M2)

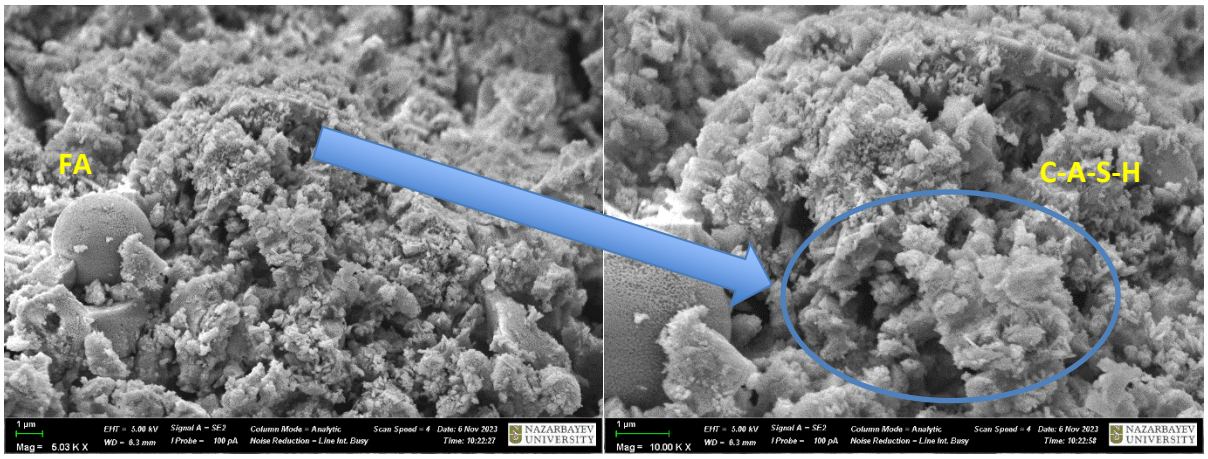

Figure 4. 19: SEM image of ambient air cured sample 75/25 (M6)

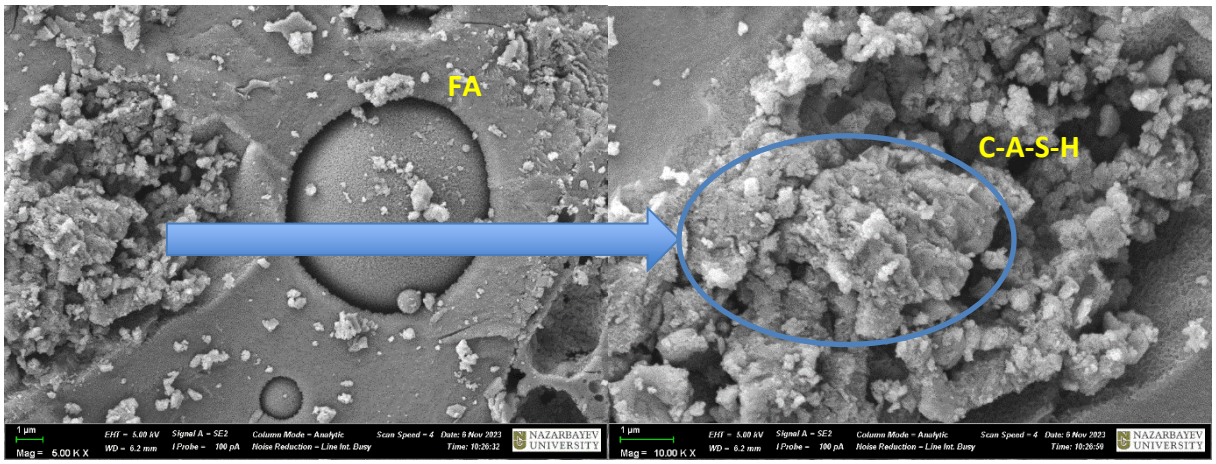

Figure 4. 20: SEM image of water cured sample 75/25 (M8)

Table 4. 1: EDS results

Element	Line	Mass, %	Atom, %
C	K	13.44±0.15	20.21±0.23
O	K	50.83±0.29	57.37±0.33
Na	K	3.38±0.07	2.66±0.06
Mg	K	1.33±0.04	0.99±0.03
Al	K	6.79±0.08	4.55±0.05
Si	K	17.36±0.13	11.16±0.08
K	K	0.33±0.02	0.15±0.01
Ca	K	6.30±0.08	2.84±0.04
Ti	K	0.23±0.02	0.09±0.01
Total		100.00	100.00

4.4.3. Fourier transform infrared spectroscopy (FTIR) analysis

Figure 4.21 shows the FTIR spectra of geopolymer mortar samples. According to Bell [98], bands in the range of 900-1000 cm^{-1} show the binding materials' absorption, consequently forming Si-O-Si and Si-O-Al asymmetric and symmetric stretching bonds in the geopolymer structure. Shift to a higher number indicates the higher compressive strength and formation of C-S-H and C-A-S-H gel in geopolymer matrix structure [96]. Thus, it can be observed that the lowest wave number band is obtained for water-cured and ambient air-cured mixtures, which correlates with the compressive strength results.

The presence of the O-C-O band in CO_2 cured samples in the range of 1450-1500 cm^{-1} represents the formation of carbonate products in the geopolymer matrix. This correlates with the findings from XRD analysis, where calcium carbonate (calcite) formation is observed.

The bond of 2300 cm^{-1} indicates the C=O bonding formation, which indicates the formation of CO_2 inside the geopolymer matrix structure. However, the curing regime and

duration show no significant differences in bond formation. The bands in the 450-500 cm^{-1} range represent the Si-O-M (M-metal) bond vibration, where the M is Fe, Mg, or Al. All mixtures have the corresponding bond due to the presence of metal cations in the matrix structure. The curing regime and duration do not affect the formation of the following bond.

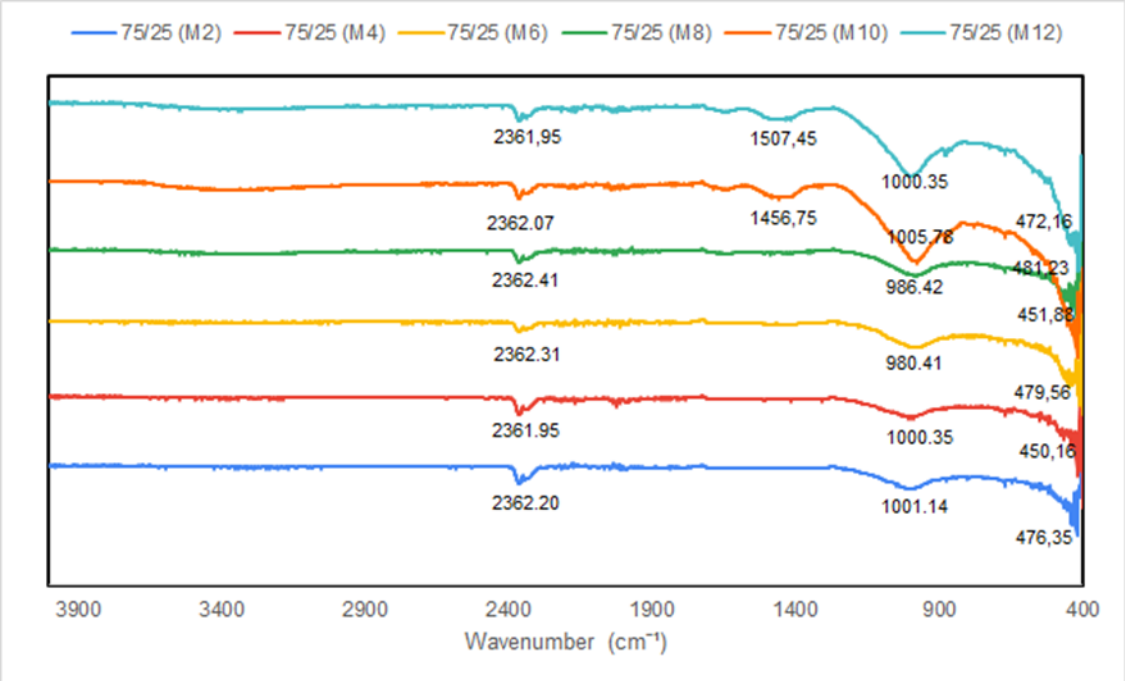

Figure 4. 21: FTIR spectra

Chapter 5 - Conclusion

The research work started from the material characterization stage. Since the key concept of the work is the utilization of basic oxygen furnace slag (BOFS) as an aggregate material for geopolymer production, its physical and chemical properties are investigated. The identified properties of BOFS further affected the geopolymer mixture proportion. The hindrance associated with BOFS as an aggregate material is the presence of free calcium oxide (f-CaO) and free magnesium oxide (f-MgO) in its components, which causes expansion problems.

This research mainly aims to study the effect of the curing regime on the properties of BOFS-based geopolymer mortar. The different BOFS to sand ratio effect is also evaluated on geopolymer properties. There are 15 mixture types, where 4 different curing regimes are studied: steam, ambient air, water, and CO_2. While the duration variation of steam curing is 6 and 12 hours, CO_2 curing is 12 and 24 hours, respectively. 3 different BOFS/sand ratios of 100/0, 75/25 and 50/50 are also compared. The test results as a whole led to the following conclusions.

- The highest relative flowability was obtained for the geopolymer mixture with a BOFS/sand ratio of 75/25, and the lowest value was obtained for the mixture with a BOFS/sand ratio of 100/0. The air content of mixtures increases with the decrease of BOFS aggregate content.
- Steam curing and the combined steam and CO_2 curing enhanced the compressive strength of the BOFS-based geopolymer mixture compared to water and ambient air-curing regimes. The longer steam-curing duration affected the compressive strength of geopolymer mortar mixtures at an early age: Compared to the 6-hour steam-cured samples, the 12-hour steam-cured samples had a greater initial compressive strength. In contrast, the steam curing duration did not affect the final compressive strength. The longer CO_2 curing duration promoted the formation of stable calcium carbonate compounds, thus enhancing the compressive strength. The highest compressive strength was observed for a 75/25 BOFS/sand ratio, and such a pattern was related to better bond interlocking.
- The steam-cured samples had a smaller decrease of dielectric constant with the time in comparison to ambient air-cured samples owing to the geopolymer matrix's electrically resistive gel rapidly developing under high curing temperature and denser structure, which informs about the continuing hydration process occurring in geopolymer matrix. The

continuous water curing supported the hydration process in the geopolymer mortar samples. Thus, the dielectric constant value of water-cured samples was highest, with negligible decrease over time. The combination of steam curing with CO_2 curing revealed a lower dielectric constant value than bare steam curing because of the adverse carbon effect on the electrical conductivity of the geopolymer. The duration of steam and CO_2 curing does not affect the dielectric constant value. The BOFS to sand ratio alteration showed a negligible effect in the change of dielectric constant value.

- Water and ambient air-cured samples exhibit the highest shrinkage strain compared to those cured under other conditions. The longer duration of steam curing results in less length and mass loss. The combination of steam and CO_2 curing reduced the shrinkage strain of 6-hour steam-cured samples. However, 12-hour steam curing combined with CO_2 do not result in significant shrinkage strain changes.
- The expansion of water-cured and ambient air-cured samples was visible on the 16^{th} day of testing in 1M NaOH solution due to the formation of unstable compounds $Ca(OH)_2$ and $Mg(OH)_2$. The CO_2 curing prevented the expansion of mortar bar samples due to the formation of stable carbonate, while the steam curing prevented expansion due to accelerating the hydration and geopolymerization process under high temperatures.
- The water expansion characteristic was not affected by the curing regime. The water expansion characteristic curve underwent smaller fluctuation for a longer steam curing duration due to a more stable structure formed under the longer hydration process. The longer CO_2 curing duration promoted the formation of stable calcium carbonate compounds, thus stabilizing the water expansion curve fluctuation of geopolymer mortar samples.
- The geopolymerization reaction was more apparent during the steam and CO_2 curing than water and air curing. Curing at elevated temperatures contributesd to forming C-S-H gel and dissolving amorphous crystalline particles. The SEM image of steam-cured samples demonstrated the homogeneously packed and dense geopolymer structure, and XRD results revealed the reduction of quartz and mullite peaks intensity, which claims that the steam curing favors the continuous chemical reaction in the geopolymer matrix. However, rapid hydration and hardening are the causes of the appearance of microcracks. In contrast to air- and water-cured samples, the FTIR analysis showed that the Si-O-Si and Si-O-Al bonds shifted to a higher wavenumber in steam- and CO2-cured samples which indicates the development of C-A-S-H and C-S-H gel within the geopolymer structure. The steam

and CO_2 curing duration did not significantly affect the microstructural properties of the geopolymer.

The further research work related to this master thesis is as follows:

- Determining the effect of BOFS/sand ratio on the setting time of BOFS-based geopolymer mortar;
- Determining the effect of curing on flexural and tensile strength of geopolymer mortar;
- Conducting the SEM, FTIR, and XRD analysis on expanded mortar samples that emerged in 1M NaOH to determine the reason for expansion.

Further room for studying is also related to the one-part geopolymer mortar, where the geopolymer mortar is prepared from solid alkali activator. A comparison of one-part and two-part geopolymer mixtures can be carried out to identify their hardened, durability, and microstructural properties. Moreover, the effect of the curing regime on one-part BOFS-based geopolymer mortar samples can be studied.

References

[1] J. L. Provis, “Alkali-activated materials,” *Cement and Concrete Research*, vol. 114, pp. 40–48, Dec. 2018, doi: https://doi.org/10.1016/j.cemconres.2017.02.009.

[2] J. Zhang, C. Shi, and Z. Zhang, “Carbonation induced phase evolution in alkali-activated slag/fly ash cements: The effect of silicate modulus of activators,” *Construction and Building Materials*, vol. 223, pp. 566–582, Oct. 2019, doi: https://doi.org/10.1016/j.conbuildmat.2019.07.024.

[3] J. Zhang, C. Shi, Z. Zhang, and Z. Ou, “Durability of alkali-activated materials in aggressive environments: A review on recent studies,” *Construction and Building Materials*, vol. 152, pp. 598–613, Oct. 2017, doi: https://doi.org/10.1016/j.conbuildmat.2017.07.027.

[4] J. Guo, Y. Bao, and M. Wang, “Steel slag in China: Treatment, recycling, and management,” *Waste Management*, vol. 78, pp. 318–330, Aug. 2018, doi: https://doi.org/10.1016/j.wasman.2018.04.045.

[5] Q. Wang, D. Wang, and S. Zhuang, “The soundness of steel slag with different free CaO and MgO contents,” *Construction and Building Materials*, vol. 151, pp. 138–146, Oct. 2017, doi: https://doi.org/10.1016/j.conbuildmat.2017.06.077.

[6] W. H. Lee, T. W. Cheng, K. Y. Lin, K. L. Lin, C. C. Wu, and C. T. Tsai, “Geopolymer Technologies for Stabilization of Basic Oxygen Furnace Slags and Sustainable Application as Construction Materials,” *Sustainability*, vol. 12, no. 12, pp. 5002–5002, Jun. 2020, doi: https://doi.org/10.3390/su12125002.

[7] S. Y. Pan, P. C. Chiang, Y. H. Chen, C. D. Chen, H. Y. Lin, and E. E. Chang, “Systematic Approach to Determination of Maximum Achievable Capture Capacity via Leaching and Carbonation Processes for Alkaline Steelmaking Wastes in a Rotating Packed Bed,” *Environmental Science & Technology*, vol. 47, no. 23, pp. 13677–13685, Nov. 2013, doi: https://doi.org/10.1021/es403323x.

[8] T. Bai, Z. Song, Y. Wu, X. Hu, and H. Bai, “Influence of steel slag on the mechanical properties and curing time of metakaolin geopolymer,” *Ceramics International*, vol. 44, no. 13, pp. 15706–15713, Sep. 2018, doi: https://doi.org/10.1016/j.ceramint.2018.05.243.

[9] K. Sun, X. Peng, Sharon Lynn Chu, S. Wang, L. Zeng, and G. Ji, “Utilization of BOF steel slag aggregate in metakaolin-based geopolymer,” *Construction and Building Materials*, vol. 300, pp. 124024–124024, Sep. 2021, doi: https://doi.org/10.1016/j.conbuildmat.2021.124024.

[10] T. Gao, L. Shen, M. Shen, F. Chen, L. Liu, and L. Gao, “Analysis on differences of carbon dioxide emission from cement production and their major determinants,” *Journal of Cleaner Production*, vol. 103, pp. 160–170, Sep. 2015, doi: https://doi.org/10.1016/j.jclepro.2014.11.026.

[11] D. Babor, D. Plian, and L. Judele, “ENVIRONMENTAL IMPACT OF CONCRETE.” Available: https://www.bipcons.ce.tuiasi.ro/Archive/161.pdf.

[12] P. K. Mehta, “Reducing the environmental impact of concrete,” *Concrete international*, vol. 23, no. 10, pp. 61-66.Available: https://ecosmartconcrete.com/docs/trmehta01.pdf.

[13] R. McCaffrey, "Climate change and the cement industry," *Global cement and lime magazine (environmental special issue)*, vol 15(19), 2002.

[14] M. S. Ko, Y. L. Chen, and J. H. Jiang, "Accelerated carbonation of basic oxygen furnace slag and the effects on its mechanical properties," *Construction and Building Materials*, vol. 98, pp. 286–293, Nov. 2015, doi: https://doi.org/10.1016/j.conbuildmat.2015.08.051.

[15] Economics Committee, "Steel Statistical Yearbook," *World Steel Association: Brussels, Belgium*, 2016.

[16] B. E. Sawe, "Top 10 Steel Producing Countries in The World," *World Atlas*, Aug. 8, 2016.

[17] J. Liu and D. Wang, "Influence of steel slag-silica fume composite mineral admixture on the properties of concrete," *Powder Technology*, vol. 320, pp. 230–238, Oct. 2017, doi: https://doi.org/10.1016/j.powtec.2017.07.052.

[18] P. S. Humbert and J. Castro-Gomes, "CO2 activated steel slag-based materials: A review," *Journal of Cleaner Production*, vol. 208, pp. 448–457, Jan. 2019, doi: https://doi.org/10.1016/j.jclepro.2018.10.058.

[19] M. Geerdes, R. Chaigneau, and O. Lingiardi, *Modern Blast Furnace Ironmaking: An Introduction (Fourth Edition, 2020)*. IOS Press, 2020. Accessed: Mar. 31, 2024. [Online]. Available: https://books.google.kz/books?hl=en&lr=&id=cy4NEAAAQBAJ&oi=fnd&pg=PR1&dq=Modern+Blast+Furnace+Ironmaking+(2nd+Editio).

[20] C. Kloppers and T. Fedotova, "Primary de-oxidation of Basic Oxygen Furnace steel by means of carbon," *Journal of the Southern African Institute of Mining and Metallurgy*, vol. 101,no.4,pp.321-328,2001, doi: https://journals.co.za/doi/epdf/10.10520/AJA0038223X_2746.

[21] S. Ndlovu, G. S. Simate, and E. Matinde, "Waste Production and Utilization in the Metal Extraction Industry (1st ed.)," *CRC Press.*, 2017, doi: https://doi.org/10.1201/9781315153896.

[22] K. J. Barker, J. R. Paules, N. Rymarchyk and R. M. Jancosko, "Oxygen steelmaking furnace mechanical description and maintenance considerations," *The AISE Steel Foundation. Steel making and refining volume*, pp. 431-474, 1998, Pittsburgh.

[23] S. Teir, S. Eloneva, C.-J. Fogelholm, and R. Zevenhoven, "Dissolution of steelmaking slags in acetic acid for precipitated calcium carbonate production," *Energy*, vol. 32, no. 4, pp. 528–539, Apr. 2007, doi: https://doi.org/10.1016/j.energy.2006.06.023.

[24] T.S. Naidu, L. D. Van Dyk, C. M. Sheridan, and D. G. Grubb, "Passive acid mine drainage remediation using BOF steel slag and sugarcane bagasse," *Protection and restoration of the environment XIV*, pp. 438-447, 2018.

[25] K. C. Mills, L. Yuan, and R. T. Jones, "Estimating the physical properties of slags," *Journal of The South African Institute of Mining and Metallurgy*, vol. 111, no. 10, pp. 649–658, Oct. 2011.

[26] "Statistics," *Euroslag*. https://www.euroslag.com/products/statistics/ (accessed Mar. 31, 2024).

[27] I. B. O. MINES "GOVERNMENT OF INDIA MINISTRY OF MINES INDIAN BUREAU OF MINES," 2016. Accessed: Mar. 31, 2024. [Online]. Available: https://ibm.gov.in/writereaddata/tenders/01022017134804TENDERFORAMCXRF.pdf

[28] Y. Xue, S. Wu, H. Hou, and J. Zha, "Experimental investigation of basic oxygen furnace slag used as aggregate in asphalt mixture," *Journal of Hazardous Materials*, vol. 138, no. 2, pp. 261–268, Nov. 2006, doi: https://doi.org/10.1016/j.jhazmat.2006.02.073.

[29] Y. Xue, H. Hou, and S. Zhu, "Adsorption removal of reactive dyes from aqueous solution by modified basic oxygen furnace slag: Isotherm and kinetic study," *Chemical Engineering Journal*, vol. 147, no. 2–3, pp. 272–279, Apr. 2009, doi: https://doi.org/10.1016/j.cej.2008.07.017.

[30] S. Z. Carvalho, F. Vernilli, B. Almeida, M. Demarco, and S. N. Silva, "The recycling effect of BOF slag in the portland cement properties," *Resources, Conservation and Recycling*, vol. 127, pp. 216–220, Dec. 2017, doi: https://doi.org/10.1016/j.resconrec.2017.08.021.

[31] İ. Akın Altun and İ. Yılmaz, "Study on steel furnace slags with high MgO as additive in Portland cement," *Cement and Concrete Research*, vol. 32, no. 8, pp. 1247–1249, Aug. 2002, doi: https://doi.org/10.1016/s0008-8846(02)00763-9.

[32] J. L. Calmon, F.A. Tristão, M. Giacometti, M. Meneguelli, M. Moratti, and J. E. S. L. Teixeira, "Effects of BOF steel slag and other cementitious materials on the rheological properties of self-compacting cement pastes," *Construction and Building Materials*, vol. 40, pp. 1046–1053, Mar. 2013, doi: https://doi.org/10.1016/j.conbuildmat.2012.11.039.

[33] Y. C. Ding, T. W. Cheng, P. C. Liu, and W. H. Lee, "Study on the treatment of BOF slag to replace fine aggregate in concrete," *Construction and Building Materials*, vol. 146, pp. 644–651, Aug. 2017, doi: https://doi.org/10.1016/j.conbuildmat.2017.04.164.

[34] T. S. Naidu, C. M. Sheridan, and L. D. van Dyk, "Basic oxygen furnace slag: Review of current and potential uses," *Minerals Engineering*, vol. 149, p. 106234, Apr. 2020, doi: https://doi.org/10.1016/j.mineng.2020.106234.

[35] D. M. Proctor *et al.*, "Physical and Chemical Characteristics of Blast Furnace, Basic Oxygen Furnace, and Electric Arc Furnace Steel Industry Slags," *Environmental Science & Technology*, vol. 34, no. 8, pp. 1576–1582, Mar. 2000, doi: https://doi.org/10.1021/es9906002.

[36] A. S. Brand and J. R. Roesler, "Steel furnace slag aggregate expansion and hardened concrete properties," *Cement and Concrete Composites*, vol. 60, pp. 1–9, Jul. 2015, doi: https://doi.org/10.1016/j.cemconcomp.2015.04.006.

[37] G. Wang, Y. Wang, and Z. Gao, "Use of steel slag as a granular material: Volume expansion prediction and usability criteria," *Journal of Hazardous Materials*, vol. 184, no. 1–3, pp. 555–560, Dec. 2010, doi: https://doi.org/10.1016/j.jhazmat.2010.08.071.

[38] J. Davidovits, “Geopolymers: Inorganic polymeric new materials,” *Journal of Thermal Analysis and Calorimetry*, vol. 37, no. 8, pp. 1633–1656, Jul. 2005, doi: https://doi.org/10.1007/bf01912193.

[39] E. Gartner, “Industrially interesting approaches to ‘low-CO2’ cements,” *Cement and Concrete Research*, vol. 34, no. 9, pp. 1489–1498, Sep. 2004, doi: https://doi.org/10.1016/j.cemconres.2004.01.021.

[40] S. K. Shill, S. Al-Deen, M. Ashraf, and W. Hutchison, “Resistance of fly ash based geopolymer mortar to both chemicals and high thermal cycles simultaneously,” *Construction and Building Materials*, vol. 239, p. 117886, Apr. 2020, doi: https://doi.org/10.1016/j.conbuildmat.2019.117886.

[41] V.D. Glukhovsky, “Soil Silicates,” Gostroiizdat Publish, Kiev, 1959.

[42] P. Duxson, A. Fernández-Jiménez, J. L. Provis, G. C. Lukey, A. Palomo, and J. S. J. van Deventer, “Geopolymer technology: the current state of the art,” *Journal of Materials Science*, vol. 42, no. 9, pp. 2917–2933, Dec. 2006, doi: https://doi.org/10.1007/s10853-006-0637-z.

[43] Z. Zhang, H. Wang, J. L. Provis, F. Bullen, A. Reid, and Y. Zhu, “Quantitative kinetic and structural analysis of geopolymers. Part 1. The activation of metakaolin with sodium hydroxide,” *Thermochimica Acta*, vol. 539, pp. 23–33, Jul. 2012, doi: https://doi.org/10.1016/j.tca.2012.03.021.

[44] M. Zhang *et al.*, “Reaction kinetics of red mud-fly ash based geopolymers: Effects of curing temperature on chemical bonding, porosity, and mechanical strength,” *Cement and Concrete Composites*, vol. 93, pp. 175–185, Oct. 2018, doi: https://doi.org/10.1016/j.cemconcomp.2018.07.008.

[45] J. T. Gourley, “Geopolymers; opportunities for environmentally friendly construction materials,” *Material 2003 Conference: Adaptive materials for modern society*, Sydney, Institute of Materials Engineering Australia, 2003.

[46] V. F. F. Barbosa and K. J. D. MacKenzie, “Thermal behaviour of inorganic geopolymers and composites derived from sodium polysialate,” *Materials Research Bulletin*, vol. 38, no. 2, pp. 319–331, Jan. 2003, doi: https://doi.org/10.1016/s0025-5408(02)01022-x.

[47] H. Xu and J. S. J. Van Deventer, “Geopolymerisation of multiple minerals,” *Minerals Engineering*, vol. 15, no. 12, pp. 1131–1139, Dec. 2002, doi: https://doi.org/10.1016/s0892-6875(02)00255-8.

[48] J. G. S. van Jaarsveld, J. S. J. van Deventer, and G. C. Lukey, “The characterisation of source materials in fly ash-based geopolymers,” *Materials Letters*, vol. 57, no. 7, pp. 1272–1280, Jan. 2003, doi: https://doi.org/10.1016/S0167-577X(02)00971-0.

[49] P. Bankowski, L. Zou, and R. Hodges, “Reduction of metal leaching in brown coal fly ash using geopolymers,” *Journal of Hazardous Materials*, vol. 114, no. 1–3, pp. 59–67, Oct. 2004, doi: https://doi.org/10.1016/j.jhazmat.2004.06.034.

[50] D. Hardjito, S. E. Wallah, D. M. J. Sumajouw, and B. V. Rangan, "Fly Ash-Based Geopolymer Concrete," *Australian Journal of Structural Engineering*, vol. 6, no. 1, pp. 77–86, Jan. 2005, doi: https://doi.org/10.1080/13287982.2005.11464946.

[51] A.D. Najmabadi, "Strength properties of fly ash based geopolymer concrete containing bottom ash," Doctoral dissertation, Universiti Teknologi Malaysia, 2012.

[52] D. Suresh, and K. Nagaraju, "Ground Granulated Blast Slag (GGBS) In Concrete – A Review," *IOSR journal of mechanical and civil engineering*, vol. 12, pp. 76-82, Aug. 2015, doi: https://doi.org/10.6084/m9.figshare.1517663.v1.

[53] F. Puertas, Martínez-RamírezS., S. Alonso, and T. Vázquez, "Alkali-activated fly ash/slag cements," *Cement and Concrete Research*, vol. 30, no. 10, pp. 1625–1632, Oct. 2000, doi: https://doi.org/10.1016/s0008-8846(00)00298-2.

[54] J.S.J. van Deventer, R. San Nicolas, I. Ismail, S. A. Bernal, D. G. Brice, and J. L. Provis, "Microstructure and durability of alkali-activated materials as key parameters for standardization," *Journal of Sustainable Cement-Based Materials*, vol. 4, no. 2, pp. 116–128, Nov. 2014, doi: https://doi.org/10.1080/21650373.2014.979265.

[55] T. Yang, X. Yao, Z. Zhang, and H. Wang, "Mechanical property and structure of alkali-activated fly ash and slag blends," *Journal of Sustainable Cement-Based Materials*, vol. 1, no. 4, pp. 167–178, Dec. 2012, doi: https://doi.org/10.1080/21650373.2012.752621.

[56] D. Hardjito, S. E. Wallah, D. M. Sumajouw, and B. V. Rangan, "On the Development of Fly Ash-Based Geopolymer Concrete," *ACI Materials Journal*, vol. 101, no. 6, 2004, doi: https://doi.org/10.14359/13485.

[57] A. B. Malkawi, M. F. Nuruddin, A. Fauzi, H. Almattarneh, and B. S. Mohammed, "Effects of Alkaline Solution on Properties of the HCFA Geopolymer Mortars," *Procedia Engineering*, vol. 148, pp. 710–717, 2016, doi: https://doi.org/10.1016/j.proeng.2016.06.581.

[58] M. Jegan, R. Annadurai, and P.R. Kannan Rajkumar, "A state of the art on effect of alkali activator, precursor, and fibers on properties of geopolymer composites," *Case Studies in Construction Materials*, vol. 18, pp. e01891–e01891, Jul. 2023, doi: https://doi.org/10.1016/j.cscm.2023.e01891.

[59] M. G. Alexander and S. Mindess, *Aggregates in Concrete*. London ; New York: Taylor & Francis, , Cop, 2005.

[60] T. K. Lohani, M. Padhi, K. P. Dash, and S. Jena, "Optimum utilization of quarry dust as partial replacement of sand in concrete," *International Journal of Applied Science and Engineering Research*, vol. 1, no. 2, Apr. 2012, doi: https://doi.org/10.6088/ijaser.0020101040.

[61] Y. G. Gencer, "Mystery of Recycling: Glass and Aluminum Examples," *Handbook of Research on Waste Management Techniques for Sustainability*, 2016. https://www.igi-global.com/chapter/mystery-of-recycling/141895

[62] M. Adaway and Y. Wang, "Recycled glass as a partial replacement for fine aggregate in structural concrete – Effects on compressive strength," *Electronic Journal of Structural*

Engineering, vol. 14, no. 1, pp. 116–122, Jan. 2015, doi: https://doi.org/10.56748/ejse.141951.

[63] I. Barišić, B. Marković, and M. Zagvozda, "Freeze–thaw resistance assessment of cement-bound steel slag aggregate for pavement structures," *International Journal of Pavement Engineering*, vol. 20, no. 4, pp. 448–457, Apr. 2017, doi: https://doi.org/10.1080/10298436.2017.1309192.

[64] M. Mastali *et al.*, "Using Carbonated BOF Slag Aggregates in Alkali-Activated Concretes," *Materials*, vol. 12, no. 8, p. 1288, Apr. 2019, doi: https://doi.org/10.3390/ma12081288.

[65] A. R. Brough and A. Atkinson, "Sodium silicate-based, alkali-activated slag mortars," *Cement and Concrete Research*, vol. 32, no. 6, pp. 865–879, Jun. 2002, doi: https://doi.org/10.1016/s0008-8846(02)00717-2.

[66] M. Koushkbaghi, P. Alipour, B. Tahmouresi, E. Mohseni, A. Saradar, and P. K. Sarker, "Influence of different monomer ratios and recycled concrete aggregate on mechanical properties and durability of geopolymer concretes," *Construction and Building Materials*, vol. 205, pp. 519–528, Apr. 2019, doi: https://doi.org/10.1016/j.conbuildmat.2019.01.174.

[67] Q. Long, Y. Liu, Q. Zhao, M. Zhou, and B. Li, "Effects of GGBFS: FA ratio and humid-heat-treating on the mechanical performance and microstructure of the steel slag-based ternary geopolymer," *Construction and Building Materials*, vol. 392, Aug. 2023, doi: https://doi.org/10.1016/j.conbuildmat.2023.131750

[68] A. M. Morsy, A. M. Ragheb, A. H. Shalan, and O. H. Mohamed, "Mechanical Characteristics of GGBFS/FA-Based Geopolymer Concrete and Its Environmental Impact," *Practice Periodical on Structural Design and Construction*, vol. 27, no. 2, May 2022, doi: https://doi.org/10.1061/(asce)sc.1943-5576.0000686.

[69] A. A. Aliabdo, A. E. M. Abd Elmoaty, and M. F. Mohamed, "Permeability indices and corrosion resistance of geopolymer and Portland cement concretes," *Magazine of Concrete Research*, vol. 70, no. 12, pp. 595–609, Jun. 2018, doi: https://doi.org/10.1680/jmacr.17.00151.

[70] S. V. Patankar, S. S. Jamkar, and Y. M. Ghugal, "EFFECT OF WATER-TO-GEOPOLYMER BINDER RATIO ON THE PRODUCTION OF FLY ASH BASED GEOPOLYMER CONCRETE," pp. 296–300, Oct. 2012, doi: https://doi.org/10.47893/ijatce.2012.1048.

[71] A. A. Adam, "The Effects of Water to Solid Ratio, Activator to Binder Ratio, and Lime Proportion on the Compressive Strength of Ambient-Cured Geopolymer Concrete," *Journal of the Civil Engineering Forum*, vol. 5, no. 2, p. 161, May 2019, doi: https://doi.org/10.22146/jcef.43878.

[72] A. M. Zeyad *et al.*, "Review on effect of steam curing on behavior of concrete," *Cleaner Materials*, vol. 3, p. 100042, Mar. 2022, doi: https://doi.org/10.1016/j.clema.2022.100042.

[73] N. Lloyd and B. Vijaya Rangan, "Geopolymer Concrete: A Review of Development and Opportunities," pp. 307–314, Jan. 2010.

[74] Y. Zheng, C. Kim, X. Jin, P. Wei, and P. Jiang, "Study on the curing reaction, dielectric and thermal performances of epoxy impregnating resin with reactive silicon compounds as new diluents," *Journal of Applied Polymer Science*, vol. 107, no. 5, pp. 3127–3136, Nov. 2007, doi: https://doi.org/10.1002/app.27502.

[75] V. V. Yewale and P. G. Nikam, "EVALUATION OF EFFICIENT TYPE OF CURING FOR GEOPOLYMER CONCRETE," *JournalNX - A Multidisciplinary Peer Reviewed Journal*, pp. 293–295, May 2018.

[76] K. Sagoe-Crentsil, T. Brown, and A. Taylor, "Drying shrinkage and creep performance of geopolymer concrete," *Journal of Sustainable Cement-Based Materials*, vol. 2, no. 1, pp. 35–42, Mar. 2013, doi: https://doi.org/10.1080/21650373.2013.764963.

[77] P. Nath, and P.K. Sarker, "Geopolymer concrete for ambient curing condition,", *In Proceedings of the Australasian structural engineering conference*, pp. 11-13, July 2012, Perth, Australia.

[78] P. Nath, P. K. Sarker, and V. B. Rangan, "Early Age Properties of Low-calcium Fly Ash Geopolymer Concrete Suitable for Ambient Curing," *Procedia Engineering*, vol. 125, pp. 601–607, 2015, doi: https://doi.org/10.1016/j.proeng.2015.11.077.

[79] K. Vijai, R. Kumutha, and B. G. Vishnuram, "Effect of types of curing on strength of geopolymer concrete," *International Journal of Physical Sciences*, vol. 5, no. 9, pp. 1419–1423, Aug. 2010, doi: https://doi.org/10.5897/ijps.9000200.

[80] Nurruddin et al., "Methods of curing geopolymer concrete: A review," *International Journal of ADVANCED AND APPLIED SCIENCES*, vol. 5, no. 1, pp. 31–36, Jan. 2018, doi: https://doi.org/10.21833/ijaas.2018.01.005.

[81] J. Temuujin, R. P. Williams, and A. van Riessen, "Effect of mechanical activation of fly ash on the properties of geopolymer cured at ambient temperature," *Journal of Materials Processing Technology*, vol. 209, no. 12–13, pp. 5276–5280, Jul. 2009, doi: https://doi.org/10.1016/j.jmatprotec.2009.03.016.

[82] A. Chouksey, M. Verma, N. Dev, I. Rahman, and Kamal Upreti, "An investigation on the effect of curing conditions on the mechanical and microstructural properties of the geopolymer concrete," *Materials Research Express*, vol. 9, no. 5, pp. 055003–055003, May 2022, doi: https://doi.org/10.1088/2053-1591/ac6be0.

[83] ASTM C511, "Standard specification for mixing rooms, moist cabinets, moist rooms, and water storage tanks used in the testing of hydraulic cements and concretes,", 2013.

[84] A. M. Neville, *Properties of concrete*. Harlow Pearson Education, 2012.

[85] Y. Nahata, N. Kholia, and T. G. Tank, "Effect of Curing Methods on Efficiency of Curing of Cement Mortar," *APCBEE Procedia*, vol. 9, pp. 222–229, 2014, doi: https://doi.org/10.1016/j.apcbee.2014.01.040.

[86] P. Termkhajornkit, T. Nawa, and K. Kurumisawa, "Effect of water curing conditions on the hydration degree and compressive strengths of fly ash–cement paste," *Cement and Concrete Composites*, vol. 28, no. 9, pp. 781–789, Oct. 2006, doi: https://doi.org/10.1016/j.cemconcomp.2006.05.018.

[87] F. Vazinram, M. Jalal, and M. Y. Foroushani, “Effect of nano ZnO_2 and lime water curing on strength and water absorption of concrete, ” *International Journal of Materials and Product Technology*, vol. 50, no. 3/4, p. 356, 2015, doi: https://doi.org/10.1504/ijmpt.2015.068556.

[88] M. Bediako, J. T. Kevern, and E. O. Amankwah, “Effect of Curing Environment on the Strength Properties of Cement and Cement Extenders,” *Materials Sciences and Applications*, vol. 06, no. 01, pp. 33–39, 2015, doi: https://doi.org/10.4236/msa.2015.61005.

[89] S. Sandybay *et al.*, “Metallurgical slag wastes into pervious geopolymer concrete stabilized with CO2 capture,” *Materials Today: Proceedings*, Aug. 2023, doi: https://doi.org/10.1016/j.matpr.2023.07.366.

[90] P. Harirchi and M. Yang, “Exploration of Carbon Dioxide Curing of Low Reactive Alkali-Activated Fly Ash,” *Materials*, vol. 15, no. 9, p. 3357, May 2022, doi: https://doi.org/10.3390/ma15093357.

[91] Q. Huang, X. S. Shi, Q. Y. Wang, and L. Tang, “The Influence of Carbonization on the Performances of Fly Ash Geopolymeric Concrete,” *Applied Mechanics and Materials*, vol. 744–746, pp. 1519–1526, Mar. 2015, doi: https://doi.org/10.4028/www.scientific.net/amm.744-746.1519.

[92] M. Beltrame, R. Alves, Roberto Luiz Dias, and Franky Bruno Witzke, “Preliminary study of the effect of carbonation curing on geopolymers,” *Revista IBRACON de Estruturas e Materiais*, vol. 17, no. 1, Jan. 2024, doi: https://doi.org/10.1590/s1983-41952024000100010.

[93] G. Kareken *et al.*, “Geopolymer as a key material to utilize basic oxygen furnace slag (BOFS) as an aggregate,” *Materials Today: Proceedings*, Oct. 2023, doi: https://doi.org/10.1016/j.matpr.2023.10.093.

[94] T. Falayi, “A comparison between fly ash- and basic oxygen furnace slag-modified gold mine tailings geopolymers,” *International Journal of Energy and Environmental Engineering*, vol. 11, no. 2, pp. 207–217, Dec. 2019, doi: https://doi.org/10.1007/s40095-019-00328-x.

[95] M. S. H. Khan, A. Castel, A. Akbarnezhad, S. J. Foster, and M. Smith, “Utilisation of steel furnace slag coarse aggregate in a low calcium fly ash geopolymer concrete,” *Cement and Concrete Research*, vol. 89, pp. 220–229, Nov. 2016, doi: https://doi.org/10.1016/j.cemconres.2016.09.001.

[96] M. Mareya, A. Bahurudeen, J. Varghese, B. S. Thomas, and Nastassia Thandiwe Sithole, “Transformation of rice husk modified basic oxygen furnace slag into geopolymer composites,” *Journal of Materials Research and Technology*, vol. 24, pp. 6264–6278, May 2023, doi: https://doi.org/10.1016/j.jmrt.2023.04.225.

[97] T. Mashifana, J. Sebothoma, and T. Sithole, “Alkaline Activation of Basic Oxygen Furnace Slag Modified Gold Mine Tailings for Building Material,” *Advances in Civil Engineering*, vol. 2021, pp. 1–11, May 2021, doi: https://doi.org/10.1155/2021/9984494.

[98] R. J. Bell and P. Dean, “Atomic vibrations in vitreous silica,” *Discussions of the Faraday Society*, vol. 50, p. 55, 1970, doi: https://doi.org/10.1039/df9705000055.

[99] M. Ezzat, H. M. Khater, and M. Abdeen, “Enhanced characteristics of alkali activated slag/grog geopolymer bricks.” International Journal of Scientific & Engineering Research, vol. 7, pp. 230-243, 2016.

[100] Z. Yunsheng, S. Wei, C. Qianli, and C. Lin, “Synthesis and heavy metal immobilization behaviors of slag based geopolymer,” *Journal of Hazardous Materials*, vol. 143, no. 1–2, pp. 206–213, May 2007, doi: https://doi.org/10.1016/j.jhazmat.2006.09.033.

[101] N. Chuewangkam, T. Nachaithong, N. Chanlek, P. Thongbai, and S. Pinitsoontorn, “Mechanical and Dielectric Properties of Fly Ash Geopolymer/Sugarcane Bagasse Ash Composites,” *Polymers*, vol. 14, no. 6, p. 1140, Mar. 2022, doi: https://doi.org/10.3390/polym14061140.

Appendix

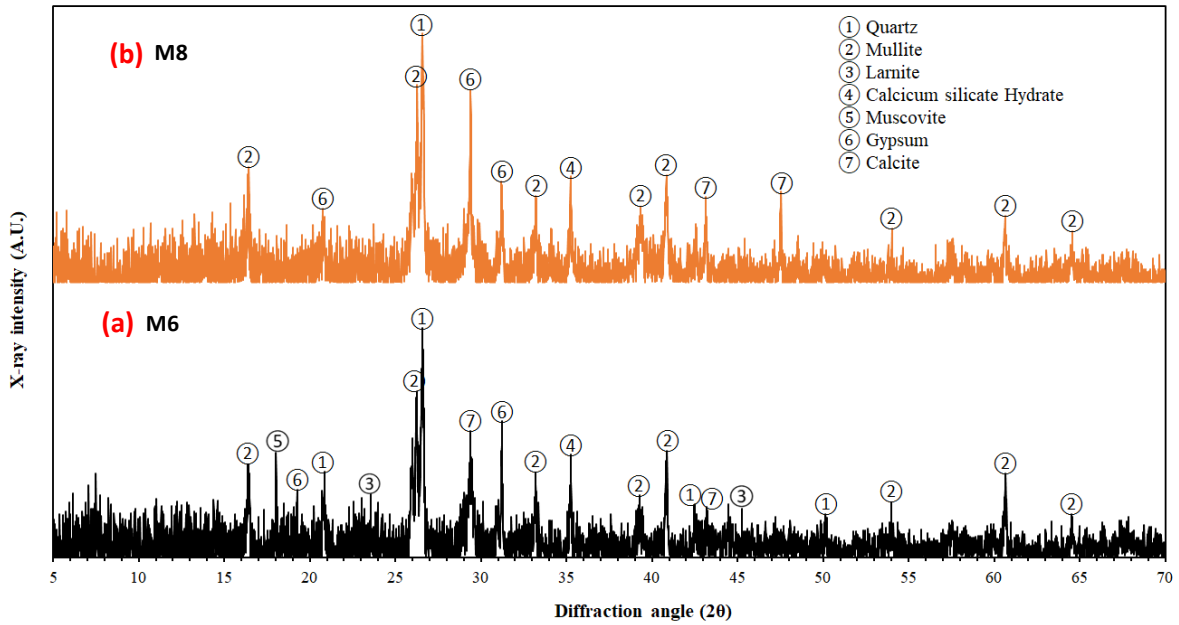

Figure 1: XRD pattern of (a) Ambient air and (b) Water cured samples

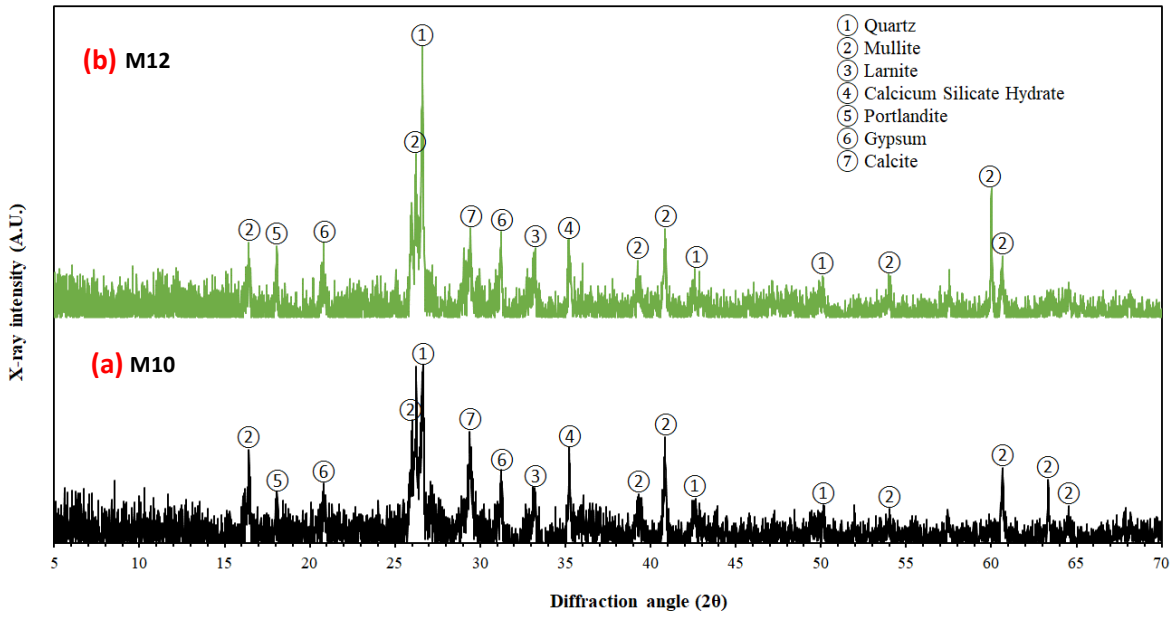

Figure 2: XRD pattern of (a) Steam cured 6hr + 6hr CO_2 and (b) Steam cured 6hr + 12hr CO_2 cured samples